(54) Title: APPARATUS AND METHOD FOR NONINVASIVE DOPPLER ULTRASOUND-GUIDED REAL-TIME CONTROL OF TISSUE DAMAGE IN THERMAL THERAPY
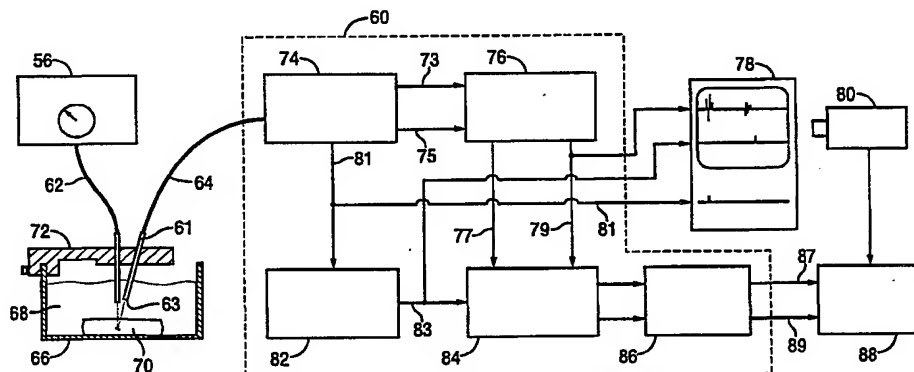
(57) Abstract

A method and apparatus for noninvasive and real-time monitoring and feedback control of the extent and geometry of tissue damage induced by various thermal modalities (laser, electromagnetic wave, ultrasound and thermistor) in different thermal therapies (hyperthermia, thermal coagulation and ablation) is provided. Unlike the existing ultrasound configurations, which use non-Doppler ultrasound techniques, the single-beam configuration in this invention employs a multiple-range-gate pulsed Doppler technique. The configuration may be operated in A-mode, M-mode, or multi-dimensional image mode to monitor tissue thermal response in the tissue being treated at multiple tissue depths along the sound beam. By measuring changes in phase (i.e., motion) and amplitude (i.e., echogenicity) of the echoes returned from the tissue under treatment, the Doppler system can determine temporal and spatial profiles of tissue temperature and the extent and geometry of tissue thermal damage. The system can also differentiate tissue responses corresponding to coagulation of tissue (in hyperthermia or coagulation treatment) versus ablation of tissue. Further, the Doppler detection provides feedback signals using fuzzy logic technology to automatically and in real-time regulate thermal output of various thermal modalities so that optimal thermal treatment can be obtained. The control of thermal output is achieved by adjusting treatment parameters such as pulse rate, exposure time and output power in the case of lasers. The Doppler detection results can also be shown on a suitable display device to allow manual feedback control of a thermal modality by a human operator.

- 1 -

DESCRIPTION
APPARATUS AND METHOD FOR NONINVASIVE DOPPLER ULTRASOUND-GUIDED REAL-TIME CONTROL OF TISSUE DAMAGE IN THERMAL THERAPY

BACKGROUND OF THE INVENTION

The present invention relates to non-invasive, real-time Doppler ultrasonic monitoring and feedback control of the extent and geometry of thermal damage in tissue treated by thermal therapy.

In recent years, thermal therapy using various modalities to thermally destroy benign and malignant lesions like tumors has gained widespread acceptance. The thermal modalities include lasers, electromagnetic wave, thermistors, and ultrasound. Thermal energy is delivered to the tissue of interest either externally or by interstitial means.

Hyperthermia is a popular thermal therapy for tumors and other tissue-related diseases. According to this method of treatment, a tumorous region inside a patient's body cavity is warmed to and kept at a temperature range of about 42° to 50° C. A number of methods of inducing hyperthermia have been tried, including electromagnetic wave (radiofrequency and microwave), whole body heating by external and extracorporeal means, and ultrasound. Hyperthermia has been applied both externally and by interstitial methods. However, with all these techniques, the problem exists of getting the energy to the target to cause the required cell death with predictability and precision, yet causing little or no damage to surrounding tissues. This problem is

- 2 -

particularly pronounced with the heating of deep seated
tumors, such as those in the liver.

Because they can be accurately focused and
5   controlled, lasers in particular have become an accepted
tool for thermal treatment (e.g., hyperthermia, tissue
coagulation and ablation). Lasers are especially suited
for thermal therapy, as they can deliver high energy
directly into the tissue being treated so as to minimize
10   the effects on surrounding normal tissue areas. The
laser energy is typically applied to the tissue of
interest through optical fibers. The optical fibers may
be introduced percutaneously, via a blood vessel, through
other body openings, or during surgical exposure of the
15   tissue.

In addition to tissue heating and thermal injury,
laser irradiation can lead to tissue vaporization,
melting, ejection, and pyrolysis, which all result in
20   removal of biological material. These effects have been
collectively described as "tissue ablation," a process
consisting of a cascade of events, each involving
threshold dependent mechanisms. Tissue ablation can also
result in charring and tearing of tissue.
25

In many thermal therapy procedures, the desire is to
coagulate and kill the tissue rather than to ablate or
vaporize it. In coagulation, the absorbed laser energy
heats cells throughout the target volume to temperatures
30   exceeding protein denaturation thresholds of
approximately 65°C. The resulting protein denaturation
induces coagulative necrosis.

Interstitial laser photocoagulation (ILP) is a
35   technique by which sufficient laser energy is deposited
at low power levels so that thermal diffusion causes
tissue coagulation while avoiding significant tissue

vaporization near the fiber tips. Coagulative necrosis is believed to occur immediately during interstitial laser treatment.

5   Accurately predicting tissue thermal damage according to theories and computer modelling is very difficult, if not impossible, and is also unreliable. This is due to the heterogeneity of tissues with respect to: (1) physical properties (e.g., optical and thermal
10   properties); (2) tissue geometry; and (3) blood perfusion in tissues. The transport of thermal energy in tissues is a complex process involving conduction, convection, radiation, metabolism, evaporation and phase change. Additionally, the broad parameter space of treatment
15   operation (energy delivered, operation duration and delivery geometry, etc.) dramatically influence the overall tissue response. All these factors result in nonuniformly distributed and highly dynamic temperature fields in tissues during thermal treatment, yielding
20   highly unpredictable tissue thermal damage.

         Thus, one of the major obstacles to effective and wide-spread applications of thermal therapies has been the lack of a reliable noninvasive and real-time
25   detection method to determine the extent and geometry of tissue damage. Such techniques can not only improve the optimization of the treatment parameters, but can also provide means for protecting critical organs surrounding treated tissues, resulting in optimal treatment.
30

         Although laser-induced damage extends deeply into the tissue, the visible effect to the naked eye is superficial. Therefore, the use of medical imaging apparatus has proved useful to evaluate tissue response
35   during thermal therapy. Indeed, imaging laser-induced damage is currently a major challenge in the field of laser medicine. The imaging modalities presently

- 4 -

available for the acquisition of clinical images include two-dimensional X-ray imaging, computed tomographic imaging (CT), magnetic resonance imaging (MRI), ultrasonography, two-dimensional radioisotope imaging,
5   single photon emission computed tomography, positron emission tomography, thermography, and transillumination. Several of these methods have been proposed for measuring temperature and detecting tissue response during laser therapy, including implanted thermistors or
10 thermocouples, CT imaging, MRI, and ultrasonic imaging.

Methods such as thermocouple or light-detector insertion can provide information about the light distribution or heat development at different points in
15 the tissue. These parameters may be used as feedback tools for laser adjustment during therapy to achieve optimal localized tumor destruction. However, the effectiveness of such probes is limited because the probes have to be placed invasively into the tissue, and
20 their position is rather critical.

The use of magnetic resonance imaging (MRI) has also been investigated as a means of visualizing tissue response during laser treatment. However, currently
25 available MRI devices require a relatively long time to collect data for an image, and thus may not be used practically for real-time evaluation. MRI devices are also large and expensive.

30 Ultrasound imaging is another technique that has gained favor of late for use in conjunction with thermal therapy. In medical ultrasound imaging, pulses of longitudinal sound waves at frequencies from 1-20 MHz are emitted by one or more piezoelectric transducers into the
35 body volume being imaged. Inside the body, ultrasound is attenuated through scattering (including reflection, refraction and diffraction) and absorption. The

intensities and arrival times of ultrasound echoes, that
is, of waves reflected back to the transducer(s) by
internal acoustic boundaries, are measured and converted
into images of the reflecting boundaries. For sound
5   waves, a boundary is a spatial discontinuity in the
acoustic impedance, defined in any medium as the product
of the speed of sound and density. The speed of sound
and acoustic impedance are temperature dependent.

10   Several investigators have reported expanding
hyperechoic regions in ultrasonic images made during
laser irradiation of tissues.   For example, hyperechoic
regions have been reported in pig liver during and after
laser irradiation. *See* Malone, *et al.*, "Sonographic
15   Changes During Hepatic Interstitial Laser
Photocoagulation: An Investigation of Three Optical
Fiber Tips," Investigative Radiology, vol. 27, pp. 804-13
(Oct. 1992); Dachman *et al.*, "US-Guided Percutaneous
Laser Ablation of Laser Tissue in a Chronic Pig Model,"
20   Radiology, vol. 176, pp. 129-33 (1990). In some cases,
it was reported that a growing hyperechoic region was
found during irradiation which sometimes became
hypoechoic after one hour. *See* Godlewski, *et al.*,
"Ultrasonic and Histopathological Correlations of Deep
25   Focal Hepatic Lesions Induced by Stereotaxic Nd-YAG Laser
Applications," Ultrasound in Med. & Biol., vol. 14, pp.
287-91 (1988); Godlewski, *et al.*, "Deep Localized
Neodymium (Nd)-YAG Laser Photocoagulation in Liver Using
a New Water Cooled and Echoguided Handpiece," Lasers in
30   Surgery and Medicine, vol. 8, pp. 501-09 (1988).
Hypoechoic regions have also been found in rat liver
after laser treatment of tumors. Van Hillegersberg, *et
al.*, "Water-Jet-Cooled Nd:YAG Laser Coagulation of
Experimental Liver Metastases: Correlation Between
35   Ultrasonography and Histology," Lasers in Surgery and
Medicine, vol. 13, pp. 332-43 (1993). Similarly,
hypoechoic regions have been found in canine myocardium

- 6 -

irradiated with a low power laser. Watanabe, *et al.*,
"Thermally Controlled Laser Irradiation of the Myocardium
with Intraoperative Ultrasound Monitoring," PACE, vol.
13, pp. 653-62 (May 1990).

5

    Because of the large increase in echogenicity which
subsequently decreases when the laser is turned off, it
has been postulated that vapor or microbubble formation
is responsible for the increase. Residual echogenicity
10   is probably related to changes in the structure and to
reorganization of tissue during coagulation and ablation.

    Air pockets created during interstitial laser
photocoagulation, either as small bubbles or a cavity at
15   the fiber tip, will generate strong ultrasound echoes.
It is thus possible to obtain ultrasound contrast images
of thermal lesions induced by thermal therapy. Further,
the use of imaging systems for potential control of
interstitial laser photocoagulation was recently
20   reviewed, with mixed results. *See* Wyman *et al.*, "Medical
Imaging Systems for Feedback Control for Interstitial
Laser Photocoagulation," Proceedings of the IEEE, vol.
80, p. 890-902 (June 1992). Both MRI and ultrasound were
able to detect changes in tissue properties during and
25   after laser irradiation. The results with ultrasound,
however, were inconsistent. It was postulated that
actual tissue vaporization (ablation) may be required to
visually observe substantial and consistent increases in
echogenicity. In addition, it appears that respiratory
30   motion poses a problem for ultrasound image-based control
of interstitial laser therapy.

    In addition to enabling visual evaluation of the
extent of thermal tissue damage, ultrasound has also been
35   used to guide placement of a laser. *See* Roth, R. and
Aretz, H., "Transurethral Ultrasound-Guided Laser-Induced
Prostatectomy (Tulip Procedure): A Canine Prostate

Feasibility Study," The Journal of Urology, vol. 146, pp.
1128-35 (Oct. 1991). Therein, a combined
ultrasound/laser device is described for transurethral
laser coagulation of the prostate. Ultrasonic images
5   were used for guidance and also for evaluating the
results of laser treatment in dogs. At higher laser
power levels (i.e., greater than 50 watts), hyperechoic
regions correlating to the area of coagulation necrosis
were seen.
10

Laser ablation of atherosclerotic plaques is another
area where real-time monitoring is needed. See Borst, et
al., "Laser Ablation and the Need for Intra-Arterial
Imaging," International Journal of Cardiac Imaging, vol.
15   4, pp. 127-33 (1989). Several investigators have used
ultrasound guidance for laser ablation of plaques with
mixed results. For example, in Aretz, et al.,
"Intraluminal Guidance of Transverse Laser Coronary
Atherectomy," International Journal of Cardiac Imaging,
20   vol. 4, pp. 153-57 (1989), the concept of a combined
laser and atherectomy and ultrasonic imaging catheter is
described. This device was subsequently evaluated for
imaging (but not lasing) in dogs. Aretz, et al.,
"Ultrasound Guidance of Laser Atherectomy," International
25   Journal of Cardiac Imaging, vol. 6, pp. 231-37 (1991).
Also, in Duda et al., "Ultrasound-Monitored Laser
Angioplasty: Preliminary Clinical Results," Cardiovasc.
Intervent. Radiol., vol. 16, pp. 89-92 (1993), a clinical
use of a combined laser angioplasty and ultrasonic
30   imaging catheter to treat femoral and iliac stenoses was
reported. The ultrasound image was found not to be
useful in directing laser ablation, but it was found
useful to measure the residual stenosis after treatment.
Cavitation bubbles were seen in the blood during
35   irradiation, but no changes in the echogenicity of the
vessel wall were noticed after laser treatment. A major
problem reported was that the ultrasound beam scanned

- 8 -

radially while the laser beam was axial to the catheter, thereby preventing real-time monitoring.

5   An ultrasonic displacement measuring system based on Doppler ultrasound principles has been described for detecting myocardial thickening. *See* Hartley, *et al.*, "An Ultrasonic Method for Measuring Tissue Displacement: Technical Details and Validation for Measuring Myocardial Thickening," IEEE Transactions on Biomedical Engineering, 10   vol. 38, pp. 735-747 (Aug. 1991), the disclosure of which is herein incorporated by reference.

The technique is based on principles of both pulse-echo and pulsed Doppler ultrasound. By detecting and 15   following the phase of the echoes returned from the transducer, the motion of the reflector with respect to the transducer can be quantified. The instantaneous phase of the returning echo is proportional to the distance of the reflector from the transducer. *See* 20   Hartley *et al.* (1991) at p. 736. Using a tone burst mode of operation, the transmitted signal (S_t) has the following form:

$$S_t = \cos(\omega t), \qquad \text{for } nT < t < nT + t_x$$
25    $$= 0 \qquad\qquad \text{elsewhere} \qquad\qquad (1)$$

where ω is the angular frequency of the transmitted wave, T is the pulse repetition period which must be an integer number of cycles of ω, n is a positive integer, and t_x is 30   the duration of the transmitted burst. This tone burst is propagated from the transducer toward a target where part of it is reflected back toward the transducer which then acts as a receiver.

35   The received echo signal (S_r) has the form

$$S_r = a \cos \{\omega(t - t_d)\}$$
$$\text{for } nT + t_d < t < nT + t_d + t_x$$
$$= 0 \quad \text{elsewhere} \tag{2}$$

where a is the amplitude of the received echo signal and t_d is the time delay between the beginning of the transmitted burst and the beginning of the received echo signal. In turn,

$$t_d = 2d/c \tag{3}$$

where d is the distance from the transducer to the reflecting interface and c is the speed of sound in the target. Rearranging and substituting results in:

$$S_r = a \cos (\omega t - 2\omega d/c), \text{ for t as in eq. (2).} \tag{4}$$

Since $\omega = 2\pi c/\lambda$, eq. **(4)** can be put in the form

$$S_r = a \cos (\omega t - \phi), \quad \text{for t as in eq. (2),} \tag{5}$$
where λ is the wavelength of the ultrasonic wave in the conducting medium (such as tissue), and where

$$\phi = 4\pi d/\lambda. \tag{6}$$

In eq. **(6)**, ϕ represents the phase (in radians) of the echo signal with respect to the transmitter signal and is directly proportional to the distance d from the transducer to the reflecting target.

A block diagram of a prior art ultrasonic displacement measuring instrument is shown in FIG. 1. In the instrument described in FIG. 1, phase is sensed by a quadrature-phase detector **32** consisting of two analog multipliers. The reference inputs to the multipliers are $\cos(\omega t)$ **[27]** and $\sin(\omega t)$ **[29]** and are derived from a master oscillator **26** which runs continuously at angular

- 10 -

frequency ω. Multiplying each of these signals by the
echo signal results in

$$\cos(\omega t) \times a \cos(\omega t - \phi)$$
$$= a\{\cos(2\omega t - \phi) + \cos(\phi)\} / 2 \qquad (7)$$

and

$$\sin(\omega t) \times a \cos(\omega t - \phi)$$
$$= a\{\sin(2\omega t - \phi) + \sin(\phi)\} / 2 \qquad (8)$$

for t as in eq. (2).

If the above signals are low-pass filtered to remove
the high frequency terms at $2\omega t$, are multiplied by 2 to
eliminate the 1/2, and are sampled only during the
received interval [i.e., t as in eq. (2)], the sampled,
phase detected signals then become

$$x = a \cos\phi \qquad (9)$$

and

$$y = a \sin\phi \qquad (10)$$

where x and y can be considered as components of a polar
coordinate phase vector of length a and angle ϕ.
Components x and y are called "quadrature range-phase
signals."

In general, the target will be moving with respect
to the transducer, which will generate a Doppler shift
and cause a rotation of the phase vector. To see how the
phase and Doppler shift frequency are related, consider a
target moving at velocity v at an angle θ with respect to
the sound beam axis. Its distance from the transducer d
is given by

$$d = \int_o^t v \cos\theta \, dt = vt \cos\theta + d_0 \qquad (11)$$

- 11 -

where d_0 is the initial position of the target. If eq.
(11) is substituted into eq. (6), phase also becomes a
function of time given by

$$\phi = (4\pi vt/\lambda) \cos \theta + \text{constant.} \tag{12}$$

Differentiating the phase yields an angular frequency
(ω_d):

$$\omega_d = d\phi/dt = (4\pi v/\lambda) \cos \theta. \tag{13}$$

Substituting $\omega_d = 2\pi f_d$ and $\lambda = c/f$, eq. (13) becomes

$$f_d = (2fv/c) \cos \theta, \tag{14}$$

which is the well-known Doppler equation with f_d being
the Doppler shift frequency, in Hz, of the reflected
wave. The Doppler shift can thus be obtained from the
phase by differentiation. For a moving target, the phase
vector rotates with an angular frequency given by ω_d in a
direction corresponding to the direction of the target
motion: clockwise for motion away from the transducer
(receding phase) or counterclockwise for motion toward
the transducer (advancing phase).

    Timing for the instrument shown in FIG. 1 (operated
at 10 MHz) is controlled by 10 MHz crystal oscillator 26.
The 10 MHz frequency is divided by 2560 by frequency
divider 14 to produce a pulse repetition frequency (PRF)
of 3.90625 kHz. A 0.4 μs pulse from pulse generator 12
is used to gate 4 cycle bursts of the 10 MHz signal [see
eq. (1)] to transmitter amplifier 28, which drives
ultrasonic transducer 10. Transducer 10 converts the
electrical signals to acoustic tone bursts, which are
propagated into the tissue where they are reflected by
structures along the sound beam. The echoes returning to
transducer 10 are converted back into electrical signals

- 12 -

[see eq. (2)], which are amplified by RF amplifier 30 to produce signal 31 (see eq. (4)) and compared by quadrature-phase detector 32 in phase to quadrature signals {cos (ωt) [27] and sin (ωt) [29]} from 10 MHz

5   oscillator 26. The two phase detector outputs 33 and 35 (which are quadrature signals that correspond to eq. (7) and (8), respectively) are then sampled by dual sample and hold circuit 34 with a 0.2 μs range-gate pulse 24 delayed by 2-50 μs from the transmit pulse by variable

10   delay circuit 18. The range of circuit 24 is selected by potentiometer 16. After sampling, the two signals are high-pass filtered at 1 Hz to remove the dc components from the stationary structures and low-pass filtered at 1 kHz by dual filters 36 to remove residual signals.

15   Except for the lower bandwidth, the sampled, filtered signals 37 and 39 are the in-phase (I) and quadrature-phase (Q) Doppler signals (which correspond to eq. (9) and (10), respectively). Signals 37 and 39 resemble quadrature audio signals from a pulsed Doppler instrument

20   for measuring blood flow, and may be received at output 52.

The vector representation of the quadrature signals may be shown in X-Y display 54 shown in FIG. 1. The

25   radius a represents the amplitude of the echo from the target, and the phase ϕ of the echo represents the position of the target. The change in position (or displacement) can be measured by noting the direction (clockwise or counterclockwise) and counting the

30   revolutions of the vector. Each revolution corresponds to reflector motion of 0.075 mm at 10 MHz. To improve the resolution of the instrument to 0.019 mm, revolutions are counted in 90° increments corresponding to axis crossings in the X-Y display 54. Logic circuits in up-

35   down counter controller 40 detect positive and negative zero crossings of each quadrature signal, assign a direction based on the polarity of the zero crossing and

- 13 -

the polarity of the other signal at the time, and
increment or decrement 8-bit up-down counter **40**. Full-
scale range for the 8-bit counter shown is about 4.8 mm.
Digital-to-analog converter (DAC) **44** receives 8-bit

5   output **42** from counter **40** and produces a voltage output
46 that represents the change in position of echoes
within the sample volume with a calibration of 2 V/mm.
Since no filter is used on displacement output **46**, it is
updated after each sample (approximately 4 kHz) whenever

10   the reflector has moved 0.019 mm.

       Signals available from the instrument shown in FIG.
1 include: displacement **46** at 2 V/mm, analog range **20** at
0.1 V/cm, quadrature signals **52**, and quadrature audio **52a**

15   from audio amplifier **50** and speaker **48**. In addition,
monitor outputs **21**, **25**, and **33** for oscilloscope **22** are
provided from transmit pulse generator **12** (for
triggering), range-gate pulse generator **24**, and phase
detector **32**, respectively. Controls are a 2-40 mm range-

20   gate potentiometer **16** and a 6, 7, or 8 bit limit switch
41 to up/down counter **40**. Inputs are from a 10 MHz
piezoelectric transducer **10** attached or planted within
the tissue of interest, and a reset command **55** from a
triggered event.

25

       No provision is made in the prior art circuit of
FIG. 1, however, for real-time evaluation of the signals
received by transducer **10** in relation to tissue thermal
response, nor of controlling the extent or geometry of

30   tissue thermal damage resulting from thermal treatment of
a lesion in living tissue. Thus, a need exists for an
apparatus and method for noninvasive, real-time
monitoring and control of the extent and geometry of
tissue damage in thermal therapies.

35

- 14 -

SUMMARY OF THE INVENTION

The problems outlined above are addressed by the
apparatus and method of the present invention. That is,
the purposes of the present invention are: (1) to
provide a noninvasive, reliable and inexpensive technique
that can monitor in real time the extent and geometry of
thermal damage and temperature profile in tissues induced
by various forms of thermal therapy; and (2) to utilize
the signal provided by such a technique as a feedback
signal to automatically or manually regulate modulation
parameters of various thermal modalities, thereby
controlling thermal output in various thermal treatment
procedures.

The present invention broadly comprises a single-
beam Doppler ultrasound configuration based on the
principles described above. In one embodiment, a laser
fiber optic is incorporated into an ultrasound transducer
with the sound and laser beams collinear. In another
preferred embodiment, the transducer is separate from the
thermal modality, which may be a laser, a thermistor, or
other thermal treatment instrument. Unlike previously
described non-Doppler ultrasound configurations, which
produce only a two-dimensional visual image of the
treatment site for visual inspection, this ultrasonic
Doppler configuration may be operated in A-mode, M-mode,
or multi-dimensional image mode to allow measurement of
echogenicity and motion in tissue along the sound beam
produced by the transducer. Furthermore, the present
invention uses the ultrasonic Doppler signals to
automatically regulate modulation parameters (such as
pulse rate, exposure time and output power of a laser or
other thermal modality) so that desired thermal treatment
can be achieved without damaging critical organs
surrounding treated tissues. The Doppler signals can

- 15 -

also be displayed on a monitor to allow manual feedback
control of the treatment parameters by a human operator.

5   The method for ultrasonic Doppler detection of
tissue response to thermal therapy according to the
present invention broadly comprises providing an echo-
Doppler transmitter/receiver coupled to a transducer,
emitting ultrasonic waves from the transducer toward the
region of a tissue receiving thermal therapy, receiving
10   echoes from the thermally treated tissue, and converting
the echoes to electrical echo signals, where the echo
signals each contain a phase vector. The x and y
components of the phase vector of each echo signal are
derived as functions of range and time. The x and y
15   components are sampled to produce multiple pairs of I and
Q Doppler signals indicating motion and echogenicity of
the tissue relative to the transducer at a plurality of
tissue depths. The I and Q Doppler signals are then
evaluated to determine the spatial profile of tissue
20   temperature and the extent and geometry of tissue damage
resulting from said thermal therapy. The evaluation
results may be displayed for visual inspection and
evaluation.

25   Evaluation of the Doppler signals comprises
eliminating background signals in I and Q Doppler signals
to produce background-motion-free I and Q Doppler signals
and processing the background-motion-free I and Q Doppler
signals to produce current dominant shift Doppler
30   frequencies and accumulated dominant Doppler frequencies.
The current dominant shift Doppler frequencies and
accumulated dominant Doppler frequencies are then used to
produce tissue temperature reading at multiple tissue
depths and a reading indicating the extent and geometry
35   of tissue thermal damage. A current tissue irreversible
damage front is then determined from the tissue
temperature reading and from the extent and geometry of

tissue thermal damage and is compared to a user-desired
tissue irreversible damage front to produce a modulation
signal for regulating the modulation parameters, thus
controlling thermal output of the thermal modality.

5

An apparatus for ultrasonic Doppler monitoring of
the extent and geometry of tissue damage resulting from
thermal therapy according to the present invention
comprises an echo-Doppler transmitter/receiver for
10 emitting ultrasonic waves toward the region of a tissue
receiving thermal therapy, for receiving echoes from the
treated tissue, and for converting the echoes to
electrical signals, where the electrical signals each
contain a phase vector. The echo-Doppler
15 transmitter/receiver is coupled to an echo-signal
processing means for deriving x and y components of the
phase vector of each echo signal as functions of range
and time and for outputting multiple pairs of I and Q
Doppler signals, indicating echogenicity and motion in
20 the tissue relative to the transducer at a plurality of
tissue depths. The I and Q Doppler signals are also
evaluated by several modules for determining tissue
temperature at multiple tissue depths and for determining
the geometry and the extent of tissue damage resulting
25 from said thermal therapy. The evaluation results may be
displayed on a variety of devices, including a color
monitor.

The echo-signal processing means comprises, for
30 example, a quadrature-phase detector coupled to the echo-
Doppler transmitter/receiver for outputting x and y
Doppler signals, a delayed pulse generator coupled to the
echo-Doppler transmitter/receiver for producing range-
gate pulses, a dual sample/hold circuit coupled to the
35 quadrature-phase detector and the pulse generator for
receiving x and y Doppler signals and range-gate pulses
and for producing multiple pairs of I and Q Doppler

- 17 -

signals, and a lowpass filter coupled to receive the I
and Q Doppler signals from the dual sample/hold circuit.

The evaluating means comprises, for example, a
5   circuit coupled to the Doppler detector for receiving
pairs of I and Q Doppler signals and for eliminating
background noise in the I and Q Doppler signals to
produce background-motion-free I and Q Doppler signals.
The background-motion-free I and Q Doppler signals are
10   then processed by circuitry to produce current dominant
shift Doppler frequencies and accumulated dominant
Doppler frequencies. Fuzzy logic circuitry utilizes the
current dominant shift Doppler frequencies and
accumulated dominant Doppler frequencies to produce
15   tissue temperature readings at multiple tissue depths and
readings indicating the extent and geometry of tissue
thermal damage. The fuzzy logic circuitry also
determines a tissue irreversible damage front from the
tissue temperature and tissue thermal damage readings.
20   Finally, another fuzzy logic circuitry is used to compare
the current tissue irreversible damage front to a user-
desired tissue irreversible damage front to produce a
modulation signal for regulating the modulation
parameters of the thermal modality to achieve controlled
25   thermal output. Manual feedback control of thermal
modalities can also be achieved according to the
displayed Doppler ultrasound signals.

The present invention can be widely used to monitor
30   temporal and spatial progress of thermal damage and
tissue temperature during thermal therapies, and thus is
useful for hyperthermia, thermal coagulation and ablation
treatments.

35   The advantages of the present invention will be
further appreciated from the drawings and from the
detailed description provided below.

- 18 -

BRIEF DESCRIPTION OF THE DRAWINGS

The herein described advantages and features of the present invention, as well as others which will become
5   apparent, are attained and can be understood in more detail by reference to the following description and appended drawings, which form a part of this specification.

10   It is to be noted, however, that the appended drawings illustrate only exemplary embodiments of the invention and are therefore not to be considered limiting of its scope, for the invention may admit to other equally effective embodiments.
15

FIG. 1 is a block diagram of a prior art single-range-gate ultrasonic Doppler displacement measurement system operating at 10 MHz.

20   FIG. 2 is a block diagram of an experimental set-up of a single-range-gate pulsed Doppler detector for detecting laser-tissue interaction according to the present invention.

25   FIG. 2A illustrates a block diagram of an analog-digital hybrid eight-range-gate pulsed Doppler ultrasound system according to the present invention as connected to apparatus for displaying and recording ultrasound signals.
30

FIG. 3 is a range-phase display of echoes from beef liver before exposure to a diode laser using the experimental set up of FIG. 2.

35   FIG. 3A is a range-phase display of echoes from beef liver after 40 seconds of exposure to a diode laser at 8 watts power using the experimental set up of FIG. 2.

FIG. 3B is a range-phase display of echoes from beef liver after 80 seconds of exposure to a diode laser at 8 watts power using the experimental set up of FIG. 2.

FIG. 3C is a range-phase display of echoes from beef liver after 260 seconds of exposure to a diode laser at 8 watts power using the experimental set up of FIG. 2.

FIG. 4 is a Doppler vector display illustrating type 1 activity signals from tissue motion using the experimental set up of FIG. 2.

FIG. 4A is a Doppler vector display illustrating random type 2 activity signals from tissue motion using the experimental set up of FIG. 2.

FIG. 4B is a Doppler vector display illustrating periodic type 2 activity signals from tissue motion using the experimental set up of FIG. 2.

FIG. 5 is a plot of Doppler amplitude versus time during one minute exposure of beef liver at 8 watts laser power using the experimental set up of FIG. 2.

FIG. 6 is a plot of residual increase in echogenicity versus laser power for exposure of beef liver using the experimental set up of FIG. 2.

FIG. 6A is a plot of delay to the start of type 2 activity versus laser power for exposure of beef liver using the experimental set up of FIG. 2.

FIG. 6B is a plot of lesion severity versus laser power for exposure of beef liver using the experimental set up of FIG. 2.

FIG. 7 is a plot of lesion severity versus residual increase in echogenicity for exposure of beef liver using the experimental set up of FIG. 2.

5   FIG. 7A is a plot of lesion severity versus delay to start of type 2 activity for exposure of beef liver using the experimental set up of FIG. 2.

FIG. 8 is a schematic diagram of the experimental
10   setup for evaluating motion detection sensitivity of the eight-range-gate pulsed Doppler detector.

FIG. 9, FIG 9A, FIG. 9B, FIG. 9C, FIG. 9D, FIG. 9E, FIG. 9F, FIG. 9G show one set of the results obtained in
15   motion detection sensitivity experiments conducted using the apparatus of FIG. 8 showing, in X-Y plots, how the I and Q Doppler signals at the eight different tissue depths changed with time. FIG. 9, FIG 9A, FIG. 9B, FIG. 9C, FIG. 9D, FIG. 9E, FIG. 9F, FIG. 9G correspond to
20   range gates 1 to 8, respectively.

FIG. 10, FIG 10A, FIG. 10B, FIG. 10C, FIG. 10D, FIG. 10E, FIG. 10F, FIG. 10G show the corresponding phase change with respect to time for the results shown in FIG.
25   9, FIG 9A, FIG. 9B, FIG. 9C, FIG. 9D, FIG. 9E, FIG. 9F, FIG. 9G. FIG. 10, FIG 10A, FIG. 10B, FIG. 10C, FIG. 10D, FIG. 10E, FIG. 10F, FIG. 10G correspond to range gates 1 to 8, respectively.

30   FIG. 11 illustrates a block diagram of the experimental setup for detecting thermal response in a fresh sample of beef muscle being heated by a thermistor according to the present invention.

35   FIG. 12, FIG 12A, FIG. 12B, FIG. 12C, FIG. 12D, FIG. 12E, FIG. 12F, FIG. 12G show trajectories of phase vectors three-dimensionally at eight tissue depths for

- 21 -

the experimental set up of FIG. 11, with the thermistor
operated at 45°C. FIG. 12, FIG 12A, FIG. 12B, FIG. 12C,
FIG. 12D, FIG. 12E, FIG. 12F, FIG. 12G correspond to
range gates 1 to 8, respectively.

5

FIG. 13, FIG 13A, FIG. 13B, FIG. 13C, FIG. 13D, FIG.
13E, FIG. 13F, FIG. 13G show trajectories of phase
vectors three-dimensionally at eight tissue depths for
the experimental set up of FIG. 11, with the thermistor
10   operated at 75°C. FIG. 13, FIG 13A, FIG. 13B, FIG. 13C,
FIG. 13D, FIG. 13E, FIG. 13F, FIG. 13G correspond to
range gates 1 to 8, respectively.

FIG. 14 illustrates a block diagram of the
15   experimental setup for detecting thermal response in the
fresh canine liver sample being irradiated by a laser
using the ultrasound system of FIG. 2A.

FIG. 15, FIG 15A, FIG. 15B, FIG. 15C, FIG. 15D, FIG.
20   15E, FIG. 15F, FIG. 15G show trajectories of phase
vectors three-dimensionally at eight tissue depths for
the experimental set up of FIG. 14. FIG. 15, FIG 15A,
FIG. 15B, FIG. 15C, FIG. 15D, FIG. 15E, FIG. 15F, FIG.
15G correspond to range gates 1 to 8, respectively.

25

FIG. 16 is a block diagram of apparatus for
noninvasive, Doppler ultrasound-guided real-time
automatic control of the extent and geometry of tissue
damage in thermal therapy according to the present
30   invention.

FIG. 17 illustrates a combined laser fiber optic and
ultrasound transducer according to the present invention.

35   FIG. 18 is a block diagram of a tissue background
signal elimination module for the apparatus shown in FIG.
16.

- 22 -

FIG. 19 is a block diagram of a Doppler signal processing module for the apparatus shown in FIG. 16.

FIG. 20 is a block diagram of a tissue temperature and thermal damage determination module for the apparatus shown in FIG. 16.

FIG. 21 is a block diagram of a laser control module for the apparatus shown in FIG. 16.

EXPERIMENTAL RESULTS

The structure and operation of apparatus according to the present invention can be appreciated by reference to the following experimental results.

1.   Experimental Results Using a Single-Range-Gate Pulsed Doppler Detector

Pulsed Doppler detector **60** shown in FIG. 2 comprises 1 mm ultrasound transducer **64** coupled to 20 MHz Doppler transmitter/receiver **74**, which was used experimentally to analyze the amplitude and phase of echoes along the laser beam generated by laser **56** through optical fiber **62** before, during, and after laser irradiation of tissue **70** *in-vitro*. The 20 MHz Doppler transmitter/receiver **74** for sensing motion in tissue was based on the 10 MHz ultrasonic displacement measurement system shown in FIG. 1, as described in Hartley, *et al.* (1991) and *supra*. The components **38, 40** and **44** in FIG. 1 were not needed. The modifications made to convert the system of FIG. 1 from a 10 MHz system to a 20 MHz system will be apparent to those of skill in the art.

The studies were done in-vitro using fresh lean beef steak (muscle) and liver (tissue **70**) submerged in water **68** in tank **66** using the apparatus as shown in FIG 2.

- 23 -

Fiber optic 62 (600μ in diameter) and ultrasound
transducer 64 were fixed in holder 72 with their tips
about 5 mm above the surface of the tissue 70 and angled
at 8° so that the beams intersected slightly below the
5   surface of the tissue 70. The beams were placed within
about 1 mm of each other from the surface to a depth of 5
mm. Laser 56 (805 nm diode laser from Diomed, Cambridge,
UK) was used to irradiate tissue 70 for approximately 30
to 180 seconds at calibrated power levels ranging from 4
10   to 23 watts (after compensating for fiber efficiency).
The spot size or diameter of the laser beam at the
surface of the tissue 70 was about 2 mm.

The Doppler transmitter/receiver 74 was connected to
15   a 1 mm diameter piece of piezoelectric ceramic (PZT-5A)
63 mounted to the blunted tip of a 16 gauge needle 61.
Eight cycle bursts of sound were transmitted into tissue
70 and the returning echoes 75 were processed by
quadrature-phase detector 76, which is similar to that
20   used in a pulsed Doppler velocimeter. Quadrature-phase
detector also received 20 MHz signal 73 from Doppler
transmitter/receiver 74. The outputs 77, 79 from
quadrature-phase detector 76 were the x and y components
of the phase vector as functions of range and time. The
25   phase of the echo signal is $\tan^{-1}$ (y/x) and the amplitude
is $(x^2 + y^2)^{\frac{1}{2}}$. Both outputs thus contained amplitude and
phase information, but are commonly referred to as
quadrature range-phase signals. One of the phase
detector outputs 79 was displayed on oscilloscope 78
30   along with a range-gate pulse 83 from pulse generator 82,
which was used to sample the detected echoes after a
variable time delay. Sync signal 81 from Doppler
transmitter/receiver 74 was applied as the trigger input
to oscilloscope 78.
35

The resulting outputs after sampling by dual sample
hold circuit 84 were the in-phase (I) and quadrature-

- 24 -

phase (Q) Doppler signals, which were low-pass filtered
with a bandwidth from 0 to 5 kHz by bandpass filters **86**.
The Doppler outputs extend down to DC because no high-
pass filter was used for our purpose, as is usually done
5   in other Doppler applications (*see* FIG.1). The
oscilloscope display **78** of the range-phase signal **79**
showed all the echoes along the sound beam while the
Doppler I and Q signals allowed quantification and
analysis of the echoes from a specific depth within the
10 tissue.

For each exposure, a video image of the range-phase
display and the I and Q Doppler signals (**87**, **89**,
respectively) was recorded from the selected depth on VCR
15 **88** (Panasonic AG-7355). Using a time code generator (not
shown), we also recorded the time from the beginning of
each exposure. Following exposure, the tissue **70** was
sliced open at the resulting lesion (if any) and
photographed. The photographs were enlarged to 4 times
20 actual size, and the lesions were analyzed for size and
color. The presence and size of any charred, blackened,
or dark areas were especially noted.

The video tapes were played back and the ultrasonic
25 activity at each depth was characterized into one of
three categories: type 0, no change in echo pattern from
baseline; type 1, slow changes in phase with relatively
constant amplitude; and type 2, large fluctuations in
amplitude and phase which were usually random but
30 occasionally showed some periodic structure. At each
exposure we quantified the time and depth at which types
1 and 2 activity started, the maximum depth of each type
of activity, the time to start of type 1 and 2 activity,
and whether the type 2 activity showed periodicity. At
35 the end of each exposure the change in echogenicity was
estimated by measuring the maximum amplitude of the
range-phase envelope divided by the maximum amplitude

- 25 -

before exposure. The I and Q signals at the arbitrarily
chosen depth were played back on X-Y oscilloscope **78** and
also into a Doppler spectrum analyzer (SP25A Medasonics,
Mt. View, CA) (not shown).

In general, two distinct types of activity were seen
in the ultrasound displays during laser irradiation of
the tissue. Type 1 activity was characterized by slow
variations on the range-phase display and slowly rotating
loops often changing in X-Y display of the I and Q
signals. This activity is similar to what we see with
tissue motion when measuring displacement with the device
shown in FIG. 1. Type 2 activity was more chaotic with
large amplitude fluctuations seen on the range-phase
display and random motion on the X-Y display.
Occasionally this motion became more periodic with rapid
but small ($< 2\pi$ radians) oscillations in phase seen on
the X-Y display. This activity is consistent with the
appearance and disappearance or vibration of strong
reflectors. Type 1 activity was primarily phase
modulation with a Doppler frequency of less than 1 Hz
while type 2 activity consisted of both amplitude and
phase modulation with Doppler frequency components
greater than 1 kHz and peak amplitudes more than 10 times
greater than the previous type 1 levels.

The range-phase output of a typical exposure of beef
liver is illustrated in FIG. 3, FIG. 3A, FIG. 3B, FIG.
3C. The x-axis represents tissue depth in mm, and the y-
axis represents the y range-phase signal in volts.
Before exposure, the tissue echogenicity was low, as
shown in FIG. 3. Forty seconds after turning on the
laser, the tissue activity was type 1 with slowly moving
echoes of increasing echogenicity, as shown in FIG. 3A.
At 80 seconds, the activity was type 2 with large random
fluctuations in amplitude and/or phase extending 5 μs
(3.8 mm) into the beef, as seen in FIG. 3B. As soon as

- 26 -

the laser was turned off, the tissue activity reverted to
type 1, as seen in FIG. 3C, with higher echogenicity than
before exposure. Each photograph represents one video
frame or approximately 1/30 second.

5

FIG. 4, FIG. 4A, FIG. 4B show an X-Y display of the
I and Q Doppler signals during tissue motion and type 1
activity (FIG. 4), random type 2 activity (FIG. 4A), and
periodic type 2 activity (FIG. 4B). This type of display

10   shows the locus or motion of the Doppler vector during
the time of the photograph. The amplitude is the
distance from the center, and the phase is the angle to
the X axis. The Doppler shift is the frequency of
rotation with the direction of rotation (counterclockwise

15   or clockwise) corresponding to the direction of tissue
motion (toward or away from the transducer). Because the
very slow motion of the tissues produces Doppler shifts
of less than 1 Hz, the audio bandwidth of the VCR (20 Hz
- 30 kHz) does not allow recording of type 1 signals

20   without distortion. It was also difficult to freeze a
suitable X-Y display of type 1 activity in real-time
during exposure. Therefore, the signal in FIG. 4 was
made after exposure by moving the transducer with respect
to the tissue while recording I and Q signals. Each

25   revolution of the Doppler vector corresponds to tissue
motion of 37.5 μm, and the frequency of rotation is the
Doppler shift. This display is very similar to the
slowly rotating X-Y displays seen during data acquisition
with full bandwidth to DC. With zero or low level type 1

30   activity, the vector display from recorded data shows
only a dot in the center of the display. With random
type 2 activity, the Doppler vector shows random motion
with no discernible loops as shown in FIG. 4A. During
several of the exposures exhibiting random type 2

35   activity, we recorded transient narrow-band periodic
activity as shown in FIG. 4B. The arcs are partial loops
($\approx$70°) which would correspond to back and forth motion or

- 27 -

vibration of a reflector of 0.1 wavelength or about 7
microns. Because of the 20 Hz AC coupling to the VCR,
the centroid of the arcs is not in the center of the
display.

To facilitate demonstration of the variation of the
amplitude of the Doppler signal during an exposure, the I
signal was played back through an amplitude detector
consisting of a precision full-wave rectifier followed by
a two-pole 2 Hz low-pass filter (not shown in FIG. 2).
See Hartley, *et al.*, "Doppler Quantification of Echo-
Contrast Injections *In Vivo*," <u>Ultrasound in Med. & Biol.</u>,
vol. 19, pp. 269-78 (1993), the disclosure of which is
herein incorporated by reference. FIG. 5 shows the time
course of the Doppler amplitude during a 60 second
exposure to the diode laser at 8 watts power. Again,
type 0 and type 1 activity show zero amplitude because of
bandwidth limitations of the VCR while type 2 activity
shows a high amplitude with much variability during the
first half of the exposure. During the final 25 seconds
the amplitude is fairly constant indicating steady state
activity until the laser is turned off. The transition
from type 1 to type 2 activity was usually a sudden event
occurring 2 to 104 seconds after energizing the laser.
After type 2 activity was initiated, it often increased
or decreased in intensity and usually continued until the
laser was turned off.

The data from all exposures are summarized in Table
I. Of the 35 exposures analyzed, 28 showed visible
lesions, which had blanched or light colored borders, and
most had a visibly darker core. The dimensions of the
lesions ranged from 3 to 6 mm in diameter with a core 1.5
to 3 mm diameter. The other 7 exposures showed no
visible lesion. For simplicity, the lesions were
characterized by the color of the core into 4 categories:
black, dark, faint, and none. The transition from type 1

- 28 -

to type 2 activity (22 of 35 exposures) always started at the surface of the tissue and extended to an eventual depth of 1.5 to 4.5 mm (2 to 6 μs). Transient periodic or oscillatory activity was noted at the arbitrary sample

5   volume depth in 10 of the exposures exhibiting type 2 activity. There was an increase in echo amplitude in 33 of the 35 exposures with an average increase of 5.5 fold. For those exposures showing only type 1 activity the increase was 1.9 versus 7.4 for the exposures showing

10   type 2 activity.

FIG. 6, FIG. 6A, FIG. 6B show graphs of several of the measured parameters versus laser power for liver and muscle tissue. The residual echogenicity tends to

15   increase with laser power for both liver and muscle, as shown in FIG. 6. The delay to the start of type 2 activity (if it occurred) shows a strong relationship to laser power for liver, but not for muscle in the range of power levels available, as shown in FIG. 6A. The

20   darkness of the lesion core also shows a relationship to laser power for both liver and muscle, as shown in FIG. 6B. In these graphs, the data for liver and muscle are different with both tissue damage and ultrasonic changes occurring at lower power levels for liver than for

25   muscle.

FIG. 7 and FIG. 7A show graphs of lesion severity (darkness of lesion core) versus ultrasonically derived parameters (increase in echogenicity in FIG. 7 and delay

30   to the start of type 2 activity in FIG. 7A) for liver and muscle. Both parameters seem to relate to lesion severity with a stronger relationship for the delay to the start of type 2 activity than for the increase in echogenicity. In these graphs, the points for liver and

35   muscle overlap.

- 29 -

As noted previously in this specification, several investigators have reported expanding hyperechoic regions in ultrasonic images made during laser irradiation of tissues. Because of the large increase in echogenicity

5   which subsequently decreases when the laser is turned off, it has been postulated that vapor or microbubble formation is responsible for the increase. The type 2 activity in our exposures is characterized by large and dynamic modulation in the amplitude and phase of the

10   signal as seen in FIG. 3B and FIG. 4A. The activity usually starts suddenly and stops immediately when the laser is turned off. This is most likely caused by the appearance and disappearance of highly reflective scatterers such as gas bubbles. Thus, we concluded that

15   the dynamic type 2 activity is caused by vaporization of tissue, and the residual increase in echogenicity after the laser has been turned off is due to remaining gas bubbles or to the dehydration or carbonization of the remaining tissue.

20

Both residual echogenicity and the delay to the start of type 2 activity are functions of laser power as shown in FIG. 6, FIG. 6B. The differences between muscle and liver are likely due to different absorption

25   coefficients for the 805 nm laser energy. The darker liver probably absorbed more of the applied energy, and thus lesions occurred at lower power than in muscle.

The acoustic parameters also changed at lower power

30   levels for liver than for muscle suggesting that they are related to energy absorption and/or lesion development. If type 2 activity is caused by vaporization of tissue, the delay between energizing the laser and the start of type 2 activity should be a function of the total power

35   absorbed by the tissue and the ability to dissipate the heat as the temperature rises. It is known that lesion severity and size is related to the amount of power

absorbed and the time of application. Total power
absorbed is the product of the laser power applied and
the absorption coefficient of the tissue. FIG. 7A shows
a strong relationship between lesion severity and the
5   delay to type 2 activity suggesting that this parameter
is related to the power absorbed and could be used to
predict lesion severity independent of tissue type,
color, or optical absorption properties.

10   Residual echogenicity is probably related to changes
in the structure and to reorganization of tissue during
coagulation and ablation. In this study, type 2 activity
was easy to detect, and the delay to the start was an
accurate number. Amplitude, however, was more difficult
15   to quantify accurately and reproducibly.

Periodic type 2 activity has not been reported by
others, but resembles signals we see by placing a Doppler
sample volume on the end of a wire connected to a
20   vibrating speaker (Hartley, et al. (1991), supra). If
the amplitude of the vibrations is less than 0.5
wavelengths (37.5 μm), the loops are not complete
circles, and the angle of the arc is proportional to the
peak-to-peak excursion of the target. If type 2 activity
25   is caused by creation of gas bubbles, the periodicity
could be due to resonance of stable bubbles. Vibrations
with resonant frequencies from 500 Hz to 2.5 kHz were
detected in 10 of the 22 exposures exhibiting type 2
activity. None were seen with type 1 activity. Because
30   the loops in the Doppler vector are not complete and thus
not sinusoidal, the signal will be distorted, and the
frequency will not be the same as the Doppler shift
expected for the velocity of vibration. Since we sampled
at only one range, periodicity could have occurred at
35   other positions along the sound beam in other exposures.

Type 1 activity is characterized by slowly changing
phase and amplitude and is concluded to be due to tissue
motion combined with small changes in echogenicity. This
is consistent with expansion and contraction of tissue
due to heating and with coagulation at temperature
increases insufficient to cause vaporization.

TABLE I.   Summary of Experimental Data

Laser Power Applied Watts	Exposure Duration Seconds	Maximum Type of Activity (0,1,2)	Delay to start of Type 2 Seconds	Increase in Echo Amplitude x Control	Darkness of Lesion Core (if any)
Muscle					
13	180	0	–	1	none
14	180	1	–	1.3	none
18	180	1	–	1.5	none
18	180	1	–	3.7	none
18	180	2	75	6.0	faint
22	180	2	77	10.0	faint
23	180	1	–	2.4	none

TABLE I.   Summary of Experimental Data   Continued

Laser Power Applied Watts	Exposure Duration Seconds	Maximum Type of Activity (0,1,2)	Delay to start of Type 2 Seconds	Increase in Echo Amplitude x Control	Darkness of Lesion Core (if any)
Liver					
4	60	1	-	1.7	none
4	120	1	-	1.5	none
4	120	1	-	2.0	faint
5	60	2	26	6.0	faint
5	60	2	28	5.3	faint
5	120	1	-	2.3	faint
5	120	0	-	1.5	faint
5	120	2	104	7.5	dark
6	60	1	-	1.5	none
6	60	2	18	9.0	dark
6	120	2 (osc)	36	5.0	faint
6	120	2	28	3.0	dark
6	120	2	12	4.5	dark
6	180	2 (osc)	22	1.7	dark
6	120	2	26	8.0	faint
7	120	1	-	2.0	faint
7	120	2 (osc)	7	6.0	faint
8	60	2 (osc)	2	10.0	black
8	60	2	5	7.0	dark
9	100	1	-	0.7	none
10	60	2	3	10.0	black
11	30	2	3	3.0	black
12	60	2 (osc)	5	12.0	black
13	60	(osc)	2	14.5	dark
15	60	2 (osc)	2	12.5	dark
17	60	2 (osc)	4	11.0	faint
17	60	2 (osc)	2	12.0	black
19	60	2 (osc)	2	6.0	black

2.   **Experimental Results Using an Eight-**
      Range-Gate Pulsed Doppler Detector
      a.   **The development of an analog-digital**
            hybrid multiple-range-gate pulsed Doppler
            system

The ultrasound system of FIG. 2A comprises a 1.2 mm
diameter 20 MHz ultrasound transducer **64**, analog eight-
range-gate pulsed Doppler detector **60a**, high-speed 16-
channel 12-bit A/D conversion board **91** with data
acquisition software, and digital signal analyzer **96**.

Echo-Doppler transmitter **74** generates eight cycle
bursts of ultrasound that are transmitted by transducer
64 into a target, say a sample of tissue, and the echoes
returned from the tissue are received by the same
transducer **64**. The echoes are processed by detector **60a**,
which retains both amplitude and phase information in
sound echoes, as supposed to only amplitude information
in the non-Doppler ultrasound studies. Two quadrature
Doppler range-phase signals, $x(d,t)$ **(79)** (Eq. **(9)**) and
$y(d,t)$ **(77)** (Eq. **(10)**), are produced, where d is the
range along the sound beam. The range-phase signals are
sampled after eight time delays. The sampling results in
eight pairs of orthogonal components that form eight
phase vectors reflecting activity at the eight tissue
depths. The orthogonal components can be described by:

$$I(d_i, t) = A(d_i,t) \cos(\Phi(d_i,t)) \tag{15}$$
$$Q(d_i, t) = A(d_i,t) \sin(\Phi(d_i,t)) \tag{16}$$
$$i = 1, 2, \bullet\bullet\bullet\bullet\bullet\bullet, 8$$

where t is time and d_i is the distance between the
transducer tip and the tissue depth pointed to by the i-
th range-gate pulse. $A(d_i,t)$ is the amplitude while
$\Phi(d_i,t)$ is the phase (in radians) of the received echoes
at d_i. $I(d_i,t)$ and $Q(d_i,t)$ are called in-phase (I) and
quadrature-phase (Q) Doppler signals, respectively. In

- 35 -

our detector, we made space between two consecutive range
gates equal. The position of the first range-gate pulses
and the equal space between two consecutive range-gate
pulses are adjustable.

5

For given $I(d_i,t)$ and $Q(d_i,t)$, the amplitudes and
phases of the phase vectors can be computed as:

$$A(d_i,t) = \sqrt{[I(d_i,t)]^2 + [Q(d_i,t)]^2} \qquad\qquad (16)$$

$$\Phi(d_i,t) = \tan^{-1}\left(\frac{Q(d_i,t)}{I(d_i,t)}\right). \qquad\qquad (17)$$

If $I(d_i,t)$ and $Q(d_i,t)$ are shown in eight X-Y plots (X is
10    $I(d_i,t)$ and Y is $Q(d_i,t)$), the radii are the amplitudes
$A(d_i,t)$, representing echogenicity of the tissue
reflectors, while the angles between the current
positions of the phase vectors and the x axes are the
phases $\Phi(d_i,t)$, describing the position of the
15   reflectors. If a reflector at one depth moves, its
corresponding phase vector rotates. The faster the
reflector moves, the faster its corresponding vector
rotates. With 20 MHz transducer 64 used in a preferred
embodiment of the present invention, one revolution of
20   the phase change (2π) equals 37.5 μm displacement of the
reflector. The rotation direction tells whether the
reflector is approaching or leaving the ultrasound
transducer. For the detector discussed herein,
counterclockwise rotation always means the target is
25   moving towards the transducer, and clockwise rotation
means the opposite direction.

The derivative of $\Phi(d_i,t)$ with respect to time
yields the Doppler shift. That is:

30

$$d\Phi(d_i,t)/dt = 2\pi f_d(d_i,t), \qquad\qquad (18)$$

- 36 -

with $f_d(d_i,t)$ being the Doppler shift frequency in hertz.

If a phase vector rotates in one direction and completes one circle in one second, the Doppler shift frequency is one Hz. In addition to these 16 signal outputs, the detector also outputs a range-phase signal $y(d,t)$.

This type of pulsed Doppler detector has been employed in the study of blood flow and myocardial thickening (see FIG. 1). In these applications, high-pass filters are used to remove low Doppler shift frequency components as velocity of the motion is relatively high. In the detector according to the present invention, however, these high-pass filters were not implemented because a Doppler shift frequency as low as 0 Hz (direct current level) was desired to probe any motion, no matter how slow.

Sixteen analog two-pole 50 Hz low-pass active filters **86a** were implemented to filter the 16 outputs **85** ($I(d_i,t)$, $Q(d_i,t)$, $i=1,...,8$)) for the anti-aliasing purpose, as the outputs were to be digitally sampled. Consequently, the maximum Doppler shift frequency that the detector could output was 50 Hz, representing 1.95 mm/s motion.

All 16 filtered signal outputs **89** were simultaneously sampled by high-speed 16-channel 12-bit A/D conversion board **91** (Data Translation DT2801A, MA). The effective sampling resolution was 11 bits, as one bit was used for bipolarity of the ultrasound signals. Sampling was controlled by a data acquisition software (Data Translation Global Lab™) run on a 486/33MHz based personal computer **90** (having a color monitor **92**), and the data were saved on hard disk **94** of computer **90** for off-line processing and analysis.

- 37 -

To visualize and analyze the sampled signals, we
developed a digital analyzer **96** with a graphical user
interface by utilizing MATLAB™ (The MathWorks, MA) and
its toolboxes. Analyzer **96** could effectively make any
5   desirable computation on a large data volume and display
simultaneously multiple two-dimensional and three-
dimensional graphics including trajectories of the phase
vectors shown in X-Y or X-Y-Z display. Analyzer **96** could
also perform spectral analysis and many other functions.
10

       b.   **Evaluating motion detection sensitivity of**
            the pulsed Doppler detector

    FIG. 8 depicts the setup of the motion detection
15 sensitivity experiments. A piece of sponge **70a**, used as
a tissue model, was submerged in water **68** in tank **66**.
The water provided acoustic coupling for ultrasound
transducer **64**. To create very slow relative motion
between transducer **64** and sponge **70a**, transducer **64** was
20 firmly attached to a piece of straight metal wire **104**
glued on 3" speaker **102**. Speaker **102** was driven by
digital function generator **100** (Wavetek 154) capable of
generating very low frequency (*e.g.* 0.0001 Hz) triangular
waveform. Transducer **64** was driven by speaker **102** to
25 move back and forth very slowly as if the sponge were
moving and the transducer held still. The peak-to-peak
amplitude of function generator **100** was set to 1.6 V and
the motion velocity of transducer **64** could be varied by
changing the frequency of the triangular waveform.
30

    The range-phase ultrasound signal, y(d,t), was
displayed on oscilloscope **78** along with the eight range-
gate pulses. The video image of the display, along with
the time information generated by time code generator **98**
35 (FOR•A VTG-55B, Japan), were taken by video camera **80** and
recorded on video camera recorder **88** (Panasonic AG-7355).
In this experiment, the first range-gate pulse of the

- 38 -

detector was positioned to point to 1 mm beneath the
surface of sponge **70a** while the space between two
consecutive range-gate pulses was 0.5 mm. The 16
filtered outputs **89** of detector **60a** were sampled at 10
Hz.

FIG. 9, FIG 9A, FIG. 9B, FIG. 9C, FIG. 9D, FIG. 9E,
FIG. 9F, FIG. 9G is one of the experimental results,
showing the I and Q Doppler signals, in volts, at the
eight different sponge depths as X-Y plots. The
experiment lasted 15 minutes and the frequency of the
triangular waveform was 0.004 Hz. One can see that the
relative motion was sensed at all the depths as all the
plots show circular trajectories of the phase vectors.

FIG. 10, FIG 10A, FIG. 10B, FIG. 10C, FIG. 10D, FIG.
10E, FIG. 10F, FIG. 10G depict the change in phases, in
revolutions (note one revolution = 37.5 μm), with respect
to time at the eight depths (ranges 1-8 respectively).
The phase changes were computed in terms of the initial
phases, respectively. In other words, the initial
position of the phase vectors was regarded as zero phase,
producing equal basis for distance calculation.
Integration of the phases gave the distance that
transducer **64** traveled, with the initial position of
transducer **64** when the A/D conversion **91** started being
zero distance. The phases were negative (*i.e.*, the phase
vectors were rotating clockwise). The motion changed the
direction at 624 seconds when transducer **64** reached its
maximum displacement in one direction and started to move
in the opposite direction. This can be seen in FIG. 9,
FIG 9A, FIG. 9B, FIG. 9C, FIG. 9D, FIG. 9E, FIG. 9F, FIG.
9G, where all the trajectories of the phase vectors
changed from clockwise rotation to counter-clockwise
rotation. At range gates 1 and 7, the direction change
cannot be differentiated well due to the overlap of the
trajectories of the phase vectors in both directions,

- 39 -

which would happen to all the range gates should every condition be perfect.

Slight measurement errors were observed among the range gates. The mean maximum displacement was 33.47 μm with a standard deviation of 1.78 μm, happening at a mean time of 624.2 seconds with a standard-deviation of 1.458 seconds. In 15 min (900 s), the mean and standard deviation of total two-directional displacement were 48.17 μm and 3.01 μm, respectively. The mean measured velocity of the transducer motion was 0.0535 μm/s, which gauged motion detection sensitivity of the ultrasound detector **60a**. We conclude that this eight-range-gate detector is capable of detecting a motion at least as slow as 0.0535 μm/s. One should be aware that this is not the limit sensitivity of the detection, however.

     c.   **Experiments for detecting thermal response in beef muscle samples being heated by a thermistor**

FIG. 11 shows the setup of the experiment for detecting thermal response in a fresh sample of beef muscle **70b**. Tissue **70b** was submerged in water **68** in tank **66**. Glass-coated thermistor probe **106** (Thermometrics P100, NJ) was inserted into the tissue horizontally about 3.5 mm beneath the surface of tissue **70b** to heat the tissue by direct thermal conduction. Thermistor tip **106a** was in spherical shape with a diameter of 0.9 mm. The temperature of probe **106** was measured by thermocouple **107** glued on the tip **106a**. Thermocouple **107** was connected to temperature scanner **108** (Azonix ScannerPlus, MA) that displayed the current temperature as well as sent it to feedback temperature controller **110** for maintaining a user-defined temperature. The maximum power rating of thermistor **106** was 0.1 W and, consequently, the maximum achievable tissue temperature in the experiment was 76°C.

Ultrasound transducer **64** was firmly held by holder
109 mounted on X-Y-Z position adjuster **111** that was
adjusted, while we were watching the range-phase signal
$y(d,t)$ on the oscilloscope **78**, so that thermistor tip
5   **106a** was right on the ultrasound beam path. The last
range-gate pulse was pointing to the depth where
thermistor tip **106a** was located. The space between two
consecutive range gates was 0.5 mm and, therefore, the
first range-gate pulse was pointing to slightly beneath
10   the surface of tissue **70b**. The sampling rate of the A/D
conversion was 30 Hz. Thermistor **106** was turned on 10
seconds after the A/D conversion started to collect
ultrasound signal baseline. The initial tissue
temperature sensed by thermocouple **107** was 24°C.
15

FIG. 12, FIG 12A, FIG. 12B, FIG. 12C, FIG. 12D, FIG.
12E, FIG. 12F, FIG. 12G and FIG. 13, FIG 13A, FIG. 13B,
FIG. 13C, FIG. 13D, FIG. 13E, FIG. 13F, FIG. 13G
demonstrate two of the thermistor experimental results
20   three-dimensionally. They show the trajectories of the
phase vectors at the eight depths versus time (X axis is
$I(d_i,t)$ in volts, Y axis is $Q(d_i,t)$ in volts, and Z axis
is time, t, in seconds). In FIG. 12, FIG 12A, FIG. 12B,
FIG. 12C, FIG. 12D, FIG. 12E, FIG. 12F, FIG. 12G, the
25   temperature setpoint was 45°C and it took 30 seconds for
the temperature to reach the setpoint from the initial
temperature. The thermistor was turned off at 12 minutes
and 33 seconds, three minutes before the experiment
finished. In FIG. 13, FIG 13A, FIG. 13B, FIG. 13C, FIG.
30   13D, FIG. 13E, FIG. 13F, FIG. 13G the temperature
setpoint was 75°C and it took 2 minutes and 40 seconds
for the temperature to reach the setpoint from the
initial temperature. The thermistor was turned off at 10
minutes and 20 seconds, five minutes 12 seconds before
35   the experiment finished. According to FIG. 12, FIG 12A,
FIG. 12B, FIG. 12C, FIG. 12D, FIG. 12E, FIG. 12F, FIG.
12G and FIG. 13, FIG 13A, FIG. 13B, FIG. 13C, FIG. 13D,

- 41 -

FIG. 13E, FIG. 13F, FIG. 13G, once the thermistor was
turned on, all eight phase vectors started rotating
immediately and simultaneously in counterclockwise
direction. This fact indicates that the tissue at the
5   eight depths along with the sound beam was leaving
thermistor tip **106a** or equivalently, approaching
ultrasound transducer **64**. The motion was tissue thermal
expansion. The closer a range gate was to thermistor tip
106a, the larger the motion (this is especially apparent
10   in FIG. 12, FIG 12A, FIG. 12B, FIG. 12C, FIG. 12D, FIG.
12E, FIG. 12F, FIG. 12G). The motion at the range gates
7 and 8 was the largest in both cases, indicating that
the tissue around thermistor tip **106a** was the hottest and
consequently was coagulated (in the case of 75°C) first
15   compared to the tissue at the other depths. These
results indicate that one can use the motion information
to determine tissue thermal damage status at different
tissue depths.

20   Another important observation is that a thermistor
temperature of 75°C caused significantly more motion than
a temperature of 45°C did. This can be seen if one
compares motion gate-by-gate between FIG. 12, FIG 12A,
FIG. 12B, FIG. 12C, FIG. 12D, FIG. 12E, FIG. 12F, FIG.
25   12G and FIG. 13, FIG 13A, FIG. 13B, FIG. 13C, FIG. 13D,
FIG. 13E, FIG. 13F, FIG. 13G. This result is logical as
a higher temperature causes more tissue thermal expansion
than a lower temperature does. It is concluded that
tissue temperature at different depths can be determined
30   according to the motion at different depths. In other
words, temperature temporal and spatial profiles can be
determined based on the Doppler signals.

          Finally, FIG. 12, FIG 12A, FIG. 12B, FIG. 12C, FIG.
35   12D, FIG. 12E, FIG. 12F, FIG. 12G and FIG. 13, FIG 13A,
FIG. 13B, FIG. 13C, FIG. 13D, FIG. 13E, FIG. 13F, FIG.
13G show that once the thermistor was turned off, all

- 42 -

eight phase vectors quickly and simultaneously changed
rotation direction from counterclockwise to clockwise.
This motion is tissue thermal contraction, happening once
the heating source disappears.

5

It should be pointed out that the motion pattern in
all the thermistor experiments was type 1 activity, as
defined previously in the study of using the single-
range-gate pulsed Doppler detector. This was expected as
10   the tissue temperature was relatively low (maximum 75°C)
and tissue was coagulated, not ablated.

We should emphasize that 45°C is not the lowest
limit temperature the ultrasound system can detect. It
15   is low enough, though, to show that the ultrasound system
can be used in low-temperature thermal treatment, such as
hyperthermia.

The motions seen in the thermistor experiments were
20   caused by the heat generated by the thermistor and
therefore they represented thermal response in the heated
tissue. There were slow motions at different tissue
depths. The characteristics of the motions at multiple
tissue depths, including the small velocity, the
25   directions and the concurrent occurrence and timing of
the motions with the events of turning the thermistor on
or off, indicate that the motions were tissue motions.
That is, the ultrasound signals represent tissue thermal
expansion and contraction. When the thermistor was on,
30   the tissue was expanding due to the heat. Once the
heating source was off, the tissue contracted.

We conclude that our ultrasound system can
sensitively detect tissue thermal response due to
35   temperature at least as low as 45°C generated by any
thermal modalities. As tissue thermal expansion and
contraction occur in any type of tissue in response to

heat generated by any types of thermal modalities, our
ultrasound system can be used in any type of thermal
therapy, including hyperthermia, thermal coagulation and
ablation.

5

> **d. Experiments for detecting thermal response
> in canine liver samples being irradiated
> by laser**

10   FIG. 14 depicts another embodiment of the present
invention used as the setup of the experiments involving
use of Doppler ultrasound system **60a** for detecting
thermal response in fresh samples of canine liver being
irradiated by a 1064 nm Nd:YAG laser **56**. Optical fiber
15   **112** and ultrasound transducer **64** were angled at 8°,
making the laser path and ultrasound path intersect each
other from the tissue surface to a depth of about 5 mm.
Fiber **112** and ultrasound transducer **64** were held together
by holder **109** mounted on X-Y-Z position adjuster **111**.
20   The distance between the tips of transducer **64** and fiber
112 and the surface of tissue **70c** was about 3 mm. The
laser energy was deposited through optical fiber **112** of
600 μm core diameter to tissue **70c** with a surface spot
size approximately 1.5 mm in diameter. Before the
25   experiments, the fiber efficiency was measured for
computing actually delivered laser power. The first
range gate was pointing to 1 mm beneath the tissue
surface and the space between two consecutive range gates
was 0.5 mm. The A/D sampling rate was 100 Hz and each
30   experiment lasted three minutes.

       FIG. 15, FIG 15A, FIG. 15B, FIG. 15C, FIG. 15D, FIG.
15E, FIG. 15F, FIG. 15G show one of the laser
experimental results three-dimensionally as trajectories
35   of the phase vectors at the eight tissue depths versus
time (X axis is $I(d_i,t)$ in volts, Y axis is $Q(d_i,t)$ in
volts, and Z axis is time, t, in seconds). The delivered

- 44 -

laser power was 10 W. The laser was turned on 10 seconds
after the A/D conversion was activated (the 10-second
data were obtained for generating ultrasound signal
baseline information). The laser was turned off at 120
5   seconds, one minute before the end of the experiment.

The result contains both type 1 activity and type 2
activity. Before a time of 92 seconds (which can be
determined based on plots of I versus time or Q versus
10 time, not shown), all of the phase vectors slowly rotated
in counterclockwise direction and showed slow variations
in phase and small changes in amplitude, which are the
key characteristics of type 1 activity. This kind of
behavior of the phase vectors was similar to that of the
15 phase vectors in the thermistor experiments. The
behavior represents tissue thermal expansion and
indicates that the tissue temperature was relatively low
and the tissue was being coagulated, not ablated.

20 The tissue surface along the laser beam exploded at
time 92 seconds (again, the timing can be determined
based on plots of I versus time or Q versus time, not
shown). Concurrently, the behavior of all the phase
vectors suddenly changed from type 1 activity to type 2
25 activity. That is, the phase vectors demonstrated large
variations in phase and amplitude, which are the major
characteristics of type 2 activity. Also, the amplitudes
of ultrasound signals were much larger than those before
the explosion. It is known that tissue explosion
30 requires high pressure inside the tissue generated by
high temperature and a rapid increase of temperature.
Therefore, type 2 activity represents high tissue
temperature and resulting tissue ablation.

35 Once the laser was turned off at 120 seconds, type 2
activity stopped immediately and type 1 activity resumed.
However, the rotation direction of all the phase vectors

was clockwise instead of counterclockwise, which was the
case before type 2 activity took place. These results
indicate that tissue temperature decreased quickly once
the heating source (the laser) was turned off and tissue
5   thermal contraction occurred, similarly to the behavior
of those phase vectors in the end of the thermistor
experiments.

These laser experimental results show that the
10   Doppler ultrasound system can be used to differentiate
tissue coagulation (type 1 activity) and tissue ablation
(type 2 activity) in real-time. Furthermore, the Doppler
ultrasound signals can also be employed to determine in
real-time temporal and spatial distribution of tissue
15   temperature and tissue thermal damage status.

DETAILED DESCRIPTION OF THE PREFERRED EMBODIMENTS

20   As demonstrated above, the configurations of FIG. 2
and FIG. 2A have proved to be useful in detecting tissue
thermal response and in distinguishing between two
different types of tissue response resulting from thermal
treatment. Type 1 activity was determined to be due to
25   coagulation of tissue, whereas type 2 activity was
determined to correspond to ablation of tissue. The
present invention uses essentially the configuration of
FIG. 2 (single-range-gate) and FIG. 2A (multiple-range-
gate) to determine the extent and geometry of tissue
30   thermal damage. The present invention also uses these
configurations to determine tissue temperature at
multiple depths. The damage status and tissue
temperature are used to automatically or manually control
thermal modalities.
35

A block diagram of an apparatus according to the
present invention is shown in FIG. 16. The exemplary

- 46 -

Doppler ultrasound-guided, real-time automatic control
system shown in FIG. 16 uses a laser as the thermal
modality, and comprises N-range-gates pulsed Doppler
detector 60b with ultrasound transducer 64, 16-bit 2N
5   channel high speed analog-to-digital converter 120, N
identical Tissue Background Signal Elimination Modules
122, N identical Doppler Signal Processing Modules 124
and N identical Tissue Temperature and Thermal Damage
Determination Modules 126, Laser Control Module 128 and
10   laser 56 coupled to fiber optic 62. The identical
modules run in parallel to process Doppler signals from
up to N different range gates simultaneously. Other
thermal modalities include, but are not limited to,
ultrasound, thermistors, and electromagnetic wave.
15

The detailed configuration of the N-range-gates
pulsed Doppler detector 60b is similar to the eight-
range-gate pulsed Doppler detector we have constructed,
shown in FIG. 2A, except the number of range gates is N.
20   N is an arbitrary positive integer, and larger N values
yield better spatial resolution on tissue temperature and
thermal damage profiles, but the hardware implementation
may cost more.

25   16-bit 2N-channel high-speed analog-to-digital
converter 120 converts N pairs of analog Doppler
quadrature signals 119 ($I(d_i,t)$ and $Q(d_i,t)$) to digital
format (i= 1,2,...,N, and d_i is the distance between the
tip of the ultrasound transducer to the tissue depth
30   pointed to by the i-th range gate). A sampling rate of
1,024 Hz per A/D channel is used to yield sufficient
frequency resolution in power spectrum analysis in
Doppler Signal Processing Module 124.

35   Ultrasound transducer 64 and laser fiber optic 62
may be combined as shown in FIG. 17. In this embodiment,
fiber optic 62 is inserted through a hole in ultrasound

- 47 -

transducer **64**. Fiber optic **62** and ultrasound transducer
64 are held together firmly. Depending on the thermal
therapy means selected, different types and frequencies
of ultrasound transducer **64** may be used to yield both an
adequate ultrasound detection range and an appropriate
spatial resolution. Also, different types and diameters
of fiber optic **62** may be utilized to achieve desired
thermal energy deposit in tissues.

During patient treatment, the Doppler ultrasound
signals contain not only the desired motion information
created by heat due to a thermal modality such as a
laser, but also contain undesirable artifacts introduced
by tissue background motion. The background motion
includes the tissue motion caused by heart beat, by lung
respiration, by movement of patient's body, as well as
movement of the combined ultrasound/laser transducer.
The artifacts can be suppressed effectively by
subtracting the ultrasound signal at a specific range
gate designated as a reference gate from the ultrasound
signals at different range gates. This is because the
background motion creates similar artifacts at different
range gates (*i.e.* different tissue depths). The middle
range gate can be used as the reference range gate.

The detailed structure of the Tissue Background
Signal Elimination Module is illustrated in FIG. 18. A
digital infinite-duration impulse response (IIR) lowpass
filter **130** filters the digital Doppler ultrasound signals
121. Filter **130** preferably has a very sharp cutoff
frequency at 50 Hz to eliminate any frequencies higher
than 50 Hz that remain in the Doppler signals after being
filtered by analog lowpass filters **86a** in Doppler
detector **60b**. After the suppression of artifacts using
the reference range gate, residual artifacts may remain
in the ultrasound signals, which can effectively be
removed by digital signal filtering. Two digital IIR

- 48 -

bandstop filters **134** and **134a** are needed. One of the
filters **134** eliminates the frequencies corresponding to
the tissue motion synchronizing with the heart beat
activity of the patient. The heart rate and heart
5   activity signals (electrocardiogram, or ECG for short)
137 are provided by heart activity monitor **136**. The
other filter **134a** excludes the frequencies due to the
tissue motion synchronizing with the lung respiration of
the patient. The respiration rate along with respiration
10   activity signals **139** are supplied by respiration activity
monitor **138**.

     The N Tissue Background Signal Elimination Modules
     122 output N pairs of background-motion-free I and Q
15   Doppler ultrasound signals **123** to the N identical Doppler
Signal Processing Modules **124**, the detailed structure of
which is illustrated in FIG. 19. A third-order moving
average algorithm **140** is employed to smooth the
background motion-free I and Q Doppler ultrasound signals
20   **123**. The smoothed samples are sent to sample buffer **142**,
which can hold 512 samples. Buffer **142** is filled every
0.5 seconds. Once filled, buffer **142** sends 512 samples
to ultrasound phase calculator **144** and empties buffer **142**
to hold the incoming 512 samples. The buffer operation
25   repeats every 0.5 second. Ultrasound phase calculator
144 computes instantaneous ultrasound phase according to:

$$\Phi(d_i, t_k) = \tan^{-1}(Q(d_i,t_k) / I(d_i,t_k)) \qquad (19)$$
$$(i=1, 2,\ldots,N; \; k=1, 2,\ldots512; \; t_k = \text{sampling time})$$

30   where $I(d_i,t_k)$ and $Q(d_i,t_k)$ are smoothed Doppler
quadrature I and Q signals.

     The computed instantaneous ultrasound phase data are
sent to data buffer **146**, which can hold 512 phase data.
35   Once filled with 512 data in 0.5 seconds, data buffer **146**
sends the phase data to power spectrum analyzer **148**.
Like sample buffer **142**, data buffer **146** also empties

- 49 -

itself periodically for upcoming phase data. Power
spectrum analyzer **148** performs fast Fourier transform
(FFT) on the ultrasound phase data. This results in a
power spectrum of the phase signals describing strength
5   of each Doppler shift frequency component during the 0.5
second period of time.

There are 512 Doppler shift frequency components,
from 0 Hz to 50 Hz, with an equal frequency interval
10   (frequency resolution) of 0.098 Hz (50/512 Hz). The
Doppler shift frequency that has the most strength is
found, which is then used as a dominant Doppler shift
frequency representing the dominant motion velocity at a
range gate. Integrator **150** sums all of the dominant
15   Doppler shift frequencies up to the present sampling
time. As a result, an accumulated dominant Doppler shift
frequency **125a** is obtained.

N current dominant Doppler shift frequencies **125** and
20   N accumulated dominant Doppler shift frequencies **125a** are
outputted to N identical Tissue Temperature and Thermal
Damage Determination Modules **126**, the detailed structure
of which is illustrated in FIG. 20. This module is in
essence a rule-based fuzzy logic system that correlates
25   current dominant Doppler shift frequency and accumulated
Doppler shift frequency at a range gate to the tissue
temperature and tissue thermal damage in the tissue depth
corresponding to the range gate.

30   The fuzzy logic system technology (Klir, G.J. and
Folger, T.A. (1988), "Fuzzy sets, uncertainty, and
information," Prentice Hall) has been recognized by IEEE
(The Institute of Electrical and Electronics Engineers)
as one of the three key information processing
35   technologies. The basis of fuzzy logic systems is a
fuzzy set (Zadeh, L.A., "Fuzzy sets," Information and
Control, vol. 8, pp. 338-353 (1965) that describes the

membership of an object by a number between 0 and 1, as
opposed to either 0 or 1 ("member" or "nonmember") as in
classical set theory. For example, one fuzzy set might
be "young." One might define "young" as follows: 10
5   years old is "young" with membership 1, 30 years old is
"young" with membership 0.45, and 50 years old is "young"
with membership 0.1. That is, everybody is "young" to a
degree.

10   Fuzzy logic systems employ fuzzy set theory to
emulate human expert knowledge and experience, and to
process information involving uncertainty, ambiguity and
contradiction. There have been many successful
applications of fuzzy logic systems, particularly in the
15   area of control, modeling (correlation) and pattern
recognition. *See* Lee, C.C., "Fuzzy logic in control
systems: fuzzy logic controller," IEEE Transactions on
Systems, Man and Cybernetics, vol. 20, pp. 404-435
(1990); Ying, H., McEachem, M., Eddleman, D., Sheppard,
20   L.C., "Fuzzy control of mean arterial pressure in
postsurgical patients with sodium nitroprusside
infusion," IEEE Transactions on Biomedical Engineering,
vol. 39, pp. 1060-1070 (1992), the disclosures of which
are herein incorporated by reference.
25

         The module shown in FIG. 20 is a typical fuzzy logic
system. It consists of fuzzification procedure **152**,
fuzzy logic and fuzzy inference **156**, and defuzzification
procedure **166**. The current dominant Doppler shift
30   frequency **125** and accumulated dominant Doppler shift
frequency **125a** are fuzzified in block **152** according to
the fuzzy sets on dominant Doppler shift frequency and
accumulated dominant Doppler shift frequency,
respectively, defined in block **154**. The fuzzy sets on
35   dominant Doppler shift frequency **154** are trapezoidal
shaped and are predefined with names like "very high,"
"high," "medium," "low," "very low," and "extremely low."

- 51 -

The fuzzy sets cover the entire range of dominant Doppler
shift frequencies, which is 0 to 50 Hz. The fuzzy sets
on accumulated dominant Doppler shift frequency **154** are
also trapezoidal shaped and are predefined with names
5   like "very large," "large," "medium," "small," "very
small," and "extremely small." The resulting fuzzy inputs
153 are linguistically related to tissue temperature and
thermal damage by predefined fuzzy correlation rules **158**,
which are executed in block **156** in the form:

10

IF current dominant Doppler shift frequency at i-th
range gate is "high"
AND accumulated dominant Doppler shift frequency at i-
th range gate is "very large"
15   **THEN** tissue temperature at d_i is "high"
AND tissue thermal damage at d_i is "highly likely"
irreversible.

Here "high" is a fuzzy set on tissue thermal temperature
20   and "highly likely" is a fuzzy set on tissue thermal
damage (both are predefined in "fuzzy set on tissue
temperature and thermal damage" (block **164**)). Other
fuzzy sets are "very high," "near 100°C," "modest," and
"low" to cover entire tissue temperature range; and
25   "certainly," "likely," "modestly likely" and "not likely"
for describing tissue thermal damage. The fuzzy sets
defined in blocks **159** and **164** are used in block **158** to
form the fuzzy correlation rules.

30   Histologically speaking, a tissue damage in living
animals is classified as one of two states: irreversible
damage or reversible damage. Irreversible damage is
permanent damage, which is the objective of thermal
therapy. Reversible damage is temporary damage and the
35   tissue will recover to its normal state after a period of
time.

- 52 -

A set of such fuzzy correlation rules are predefined
in **158** to cover all possible situations on tissue
temperature and thermal damage. For a treatment, a
subset of the rules is chosen for use. The selection is
5   based on information from the lesion site **161** (*e.g.* in
the liver, in the brain or in the heart, etc.) and laser
system (laser type, different fiber optics, etc.--laser
system information **159**) given by the user ("user inputs"
160) before the thermal therapy is begun. Tissue
10   characteristics knowledge base **162** transfers lesion site
information **161** to tissue characteristics **163** in block
162 and sends them to fuzzy correlation rules **158** as the
criteria of selecting the rules.

15   In module **126**, all of the chosen fuzzy correlation
rules are executed in parallel simultaneously. The fuzzy
logic AND in each rule is computed using Zadeh fuzzy
logic AND (min), and fuzzy logic OR between rules (the
relationship between rules is OR) is calculated by Zadeh
20   OR (max) ("fuzzy logic and fuzzy inference" **156**). *See*
Zadeh, L.A., "Fuzzy sets," <u>Information and Control</u>, vol.
8, pp. 338-353 (1965), the disclosure of which is herein
incorporated by reference. Furthermore, the commonly
used Mamdani's minimum inference method is used to infer
25   in each of the rules the fuzzy sets in THEN part from the
fuzzy sets in IF part ("fuzzy logic and fuzzy inference"
156). *See* Mizumoto, M., "Fuzzy Controls under Various
Fuzzy Reasoning Methods," <u>Information Sciences</u>, vol. 45,
pp. 129-151 (1988), the disclosure of which is herein
30   incorporated by reference.

The execution of the rules generates fuzzy outputs
on tissue temperature and thermal damage **157** with
memberships between 0 and 1. Fuzzy outputs **157** need to
35   be defuzzified (in "defuzzification" **166**) to a crisp
tissue temperature and a crisp likelihood of thermal
damage status in terms of irreversible damage. This can

- 53 -

be carried out by using the popular centroid defuzzifier
that computes weighted average on the fuzzy outputs **157**
with corresponding memberships. For tissue temperature,
the result of the defuzzification **166** is a crisp tissue
temperature between a few hundred degrees Celsius (the
actual temperature range is application dependent). For
thermal damage, the result is a number between 0 and 1
expressing the likelihood of irreversible damage. A
threshold of 0.5 is utilized to generate 0 (reversible
tissue damage) or 1 (irreversible tissue damage).

    N tissue temperatures **127** and N thermal damage
states **127a** are sent to pseudo-color display processor
170. User-desired tissue temperature and thermal damage
profile **168** is also fed into processor **170**. Processor
170 produces user-predefined color graphics according to
information received. The graphics are displayed in
real-time on graphic color monitor **92a**. The displayed
information can be used by a human operator of a thermal
modality to realize manual feedback control of the extent
and geometry of tissue thermal damage in thermal therapy.

    It has been proved theoretically that a fuzzy logic
system like this module **126** can correlate system inputs
to system outputs as accurately as desired, no matter how
complex the correlation is. *See* Ying, H., "Sufficient
Conditions on General Fuzzy Systems as Function
Approximations," <u>Automatica</u>, vol. 30, pp. 521-525 (March
1994). This conclusion also holds for the Laser Control
Module **128**, which is a fuzzy logic system as well.

    For real-time control of thermal therapy according
to the results of Doppler ultrasound evaluation, N tissue
temperature profiles **127** and N tissue thermal damage
profiles **127a** are sent to Laser Control Module **128** as
feedback signals. The detailed structure of Laser
Control Module **128** is illustrated in FIG. 21. Module **128**

- 54 -

is similar to a typical fuzzy logic controller, whose
structure is similar to Tissue Temperature and Thermal
Damage Determination Module **126**, although the two modules
are for quite different purposes. Tissue damage front
5   determiner **172** finds the range gate which represents the
current tissue irreversible thermal damage front **171**.
Once found, the front along with the corresponding tissue
temperature **173** are used as feedback signals for control
module **128**.
10

Without losing generality, suppose the user wants to
achieve irreversible tissue thermal damage up to tissue
depth d_N. Assume the tissue thermal damage status
indicates that the current irreversible tissue damage
15   front **171** is at d_n, where $1 < n \le N$. If $n = N$, the laser
should be turned off and the treatment is finished.
Otherwise, laser modulation parameters need to be
adjusted to cause more irreversible thermal damage so
that d_n can be equal to d_N.
20

Inputs calculator **174** calculates the input
variables:
$$d(k) = d_N - d_n(k) \tag{20}$$
$$v(k) = d(k-1) - d(k). \tag{21}$$
25   where k is a positive integer representing sampling time.
Increase of k by one is meant increase of 0.5 seconds of
time. Values $d(k)$ and $v(k)$, defined in block **178**, are
fuzzified in the "fuzzification" block **176**. As in module
126, trapezoidal fuzzy sets, such as "near zero,"
30   "small," "medium," "large" and "very large," are used for
$d(k)$ and $v(k)$. Current tissue temperature at d_n **173** is
fuzzified in the "fuzzification" block **176** by the same
fuzzy sets on tissue temperature **164** as those defined in
the Tissue Temperature and Thermal Damage Module **126**.
35   The results of the fuzzification are fuzzy inputs **181**,
which will be used with fuzzy control rules **180** in block

- 55 -

182. Fuzzy sets defined in blocks **178** and **184** are used to form fuzzy control rules in block **180**.

Fuzzy control rules **180** linguistically describe the
5   strategy of changing laser modulation parameters based on the fuzzified $d(k)$, $v(k)$ and tissue temperature (fuzzy inputs **181**). Laser system information **159** and tissue characteristics **163** from module **126** are input to select a subset of fuzzy control rules from fuzzy control rules
10   **180**. Laser modulation parameters are different for different types of lasers, and hence fuzzy sets on laser modulation parameters **184** are different. As an example, if one uses a diode laser as the thermal therapy modality, then the drive current can be used as a laser
15   modulation parameter. Output power of a diode laser increases linearly with drive current once drive current is above a small laser threshold. *See* Hecht, J., "Understanding Lasers: An Entry-Level Guide," <u>IEEE Press</u>, (New York 1992).
20

Suppose we use a diode laser. Then, we define the fuzzy sets **184** on drive current as "very small," "small," "medium," "large," "very large" and "huge." A fuzzy control rule in block **180** will look like:
25

IF $d(k)$ is "large" AND $v(k)$ is "small" AND tissue temperature at d_n is "low"
THEN drive current should be "very large."

30   Given a patient, control rules are selected according to tissue characteristics **163** and laser system information **159** that are provided by Tissue Temperature and Thermal Damage Module **126**. The fuzzy control rules are executed in parallel by the same fuzzy logic and
35   fuzzy inference method (block **182**) as those used in Tissue Temperature and Thermal Damage Module **126**. The resultant fuzzy sets on drive current (fuzzy outputs **185**)

- 56 -

with memberships are defuzzified in block **186** by a
centroid defuzzifier to yield a crisp amount of drive
current. The current is sent to laser modulator **188** to
regulate the thermal output power of laser **56** connected
5   to fiber optic **62**.

        Further modifications and alternative embodiments of
this invention will be apparent to those skilled in the
art in view of this description. For example, the laser
10   used as an exemplary thermal modality in FIG. 2, FIG. 2A,
FIG. 17 and FIG. 22 may be replaced with other suitable
thermal therapy instruments, such as thermistors,
electromagnetic wave or ultrasound. Accordingly, this
description is to be construed as illustrative only and
15   is for the purpose of teaching those skilled in the art
the manner of carrying out the invention. It is to be
understood that the forms of the invention herein shown
and described are to be taken as the presently preferred
embodiments. Various changes may be made in the shape,
20   size, and arrangement of parts. For example, equivalent
elements or materials may be substituted for those
illustrated and described herein, and certain features of
the invention may be utilized independently of the use of
other features, all as would be apparent to one skilled
25   in the art after having the benefit of this description
of the invention.

- 57 -

CLAIMS

1.   A method for ultrasonic Doppler monitoring of the
extent and geometry of tissue damage in thermal therapy,
comprising the steps of:

      providing an echo-Doppler transmitter/receiver
         coupled to a transducer;

      emitting ultrasonic waves from said transducer
         toward the region of a tissue receiving thermal
         therapy;

      receiving echoes from the thermally treated tissue;

      converting the echoes to electrical echo signals,
         said echo signals each containing a phase
         vector indicating motion and echogenicity in
         the tissue relative to the transducer at a
         plurality of tissue depths;

      deriving x and y components of the phase vector of
         each echo signal as functions of range and
         time;

      outputting pairs of in-phase and quadrature-phase (I
         and Q) Doppler signals; and

      evaluating said I and Q Doppler signals to determine
         the extent and geometry of tissue damage
         resulting from said thermal therapy.

2.   The method of claim 1, further comprising treating a
tissue with a thermal modality.

- 58 -

3.   The method of claim 2, wherein said thermal modality comprises a laser coupled to an optical fiber.

5   4.   The method of claim 3, wherein said treating step comprises:

        directing a laser beam from said optical fiber into
            a tissue;

10

        providing an ultrasonic transducer coupled to said
            echo-Doppler transmitter/receiver; and

        angling said transducer probe relative to said
15   optical fiber so that the laser beam emitted
                from said optical fiber and a sound beam
                emitted from said transducer probe will
                intersect below the surface of a tissue being
                treated with said laser.

20

5.   The method of claim 3, wherein said treating step comprises providing an ultrasonic transducer coupled to said echo-Doppler transmitter/receiver, wherein said
25   transducer has a hollow core with an optical fiber disposed therein so that a laser beam projected through said optical fiber is substantially collinear with a sound beam emitted from said ultrasonic transducer.

30

6.   The method of claim 2, wherein said evaluating step comprises:

        eliminating background signals in I and Q Doppler
35   signals to produce background-motion-free I and
                Q Doppler signals;

- 59 -

processing said background-motion-free I and Q
     Doppler signals to produce current dominant
     shift Doppler frequencies and accumulated
     dominant Doppler frequencies;

processing said current dominant shift Doppler
     frequencies and accumulated dominant Doppler
     frequencies to produce tissue temperature
     readings at multiple tissue depths and readings
     indicating the extent and geometry of tissue
     thermal damage at multiple tissue depths;

determining a tissue irreversible damage front from
     said readings indicating extent and geometry of
     tissue thermal damage; and

comparing a current tissue irreversible damage front
     to a user-desired tissue irreversible damage
     front to produce a difference signal and using
     the difference signal as well as the
     temperature of the current tissue irreversible
     damage front to produce a modulation signal for
     controlling the output of said thermal
     modality.

7.   Apparatus for ultrasonic Doppler monitoring of the
extent and geometry of tissue damage due to thermal
therapy, comprising:

an echo-Doppler transmitter/receiver for emitting
     ultrasonic waves toward the region of a tissue
     receiving thermal therapy, for receiving echoes
     from the treated tissue, and for converting the
     echoes to electrical signals, said electrical
     signals each containing a phase vector
     indicating motion and echogenicity in the

- 60 -

tissue relative to the transducer at a
plurality of tissue depths;

echo-signal processing means coupled to said echo-
Doppler transmitter/receiver for deriving x and
y components of the phase vector of each echo
signal as functions of range and time and for
outputting multiple pairs of I and Q Doppler
signals; and

evaluating means for determining the extent and
geometry of tissue damage resulting from said
thermal therapy.

8.   The apparatus of claim 7, wherein said echo-signal
processing means comprises:

a quadrature-phase detector coupled to said echo-
Doppler transmitter/receiver for outputting x
and y components of the phase vector;

a delayed-pulse generator coupled to said echo-
Doppler transmitter/receiver for producing
range-gate pulses;

a dual sample/hold circuit coupled to said
quadrature-phase detector and said pulse
generator for receiving x and y signals and
range-gate pulses and for producing multiple
pairs of I and Q Doppler signals; and

a lowpass filter coupled to receive said I and Q
Doppler signals from said dual sample/hold
circuit.

- 61 -

9.   The apparatus of claim 7, further comprising:

a transducer probe coupled to said echo-Doppler
     transmitter/receiver, said transducer
     terminating in a probe tip; and

a thermal modality for applying thermal treatment to
     a living tissue.

10.   The apparatus as recited claim 9, wherein said
thermal modality comprises a laser coupled to an optical
fiber.

11.   The apparatus as recited in claim 10, wherein said
transducer probe is angled relative to said optical fiber
so that a laser beam emitted from said laser through said
optical fiber and a sound beam emitted from said
transducer will intersect below the surface of a tissue
being treated with said laser.

12.   The apparatus as recited in claim 10, wherein said
transducer has a hollow core with an optical fiber
disposed therein so that a laser beam projected through
said optical fiber is substantially collinear with a
sound beam emitted from said ultrasonic transducer.

13.   The apparatus of claim 7, wherein said evaluating
means further comprises:

means coupled to said Doppler detector for receiving
     I and Q Doppler signals and for eliminating
     background signals in said I and Q signals to

- 62 -

produce background-motion-free I and Q Doppler
signals;

means for processing said background-motion-free I
and Q Doppler signals to produce current
dominant shift Doppler frequencies and
accumulated dominant Doppler frequencies;

means for processing said current dominant shift
Doppler frequencies and accumulated dominant
Doppler frequencies to produce tissue
temperature readings at multiple tissue depths
and readings indicating the extent and geometry
of tissue thermal damage;

means for determining a tissue irreversible damage
front from said readings indicating extent and
geometry of tissue thermal damage; and

means for comparing a current tissue irreversible
damage front to a user-desired tissue
irreversible damage front to produce a
difference signal and using the difference
signal as well as the temperature of the
current tissue irreversible damage front to
produce a modulation signal for controlling the
output of said thermal modality.

1/27

FIG. 1
(Prior Art)

2/27

FIG. 2

3/27
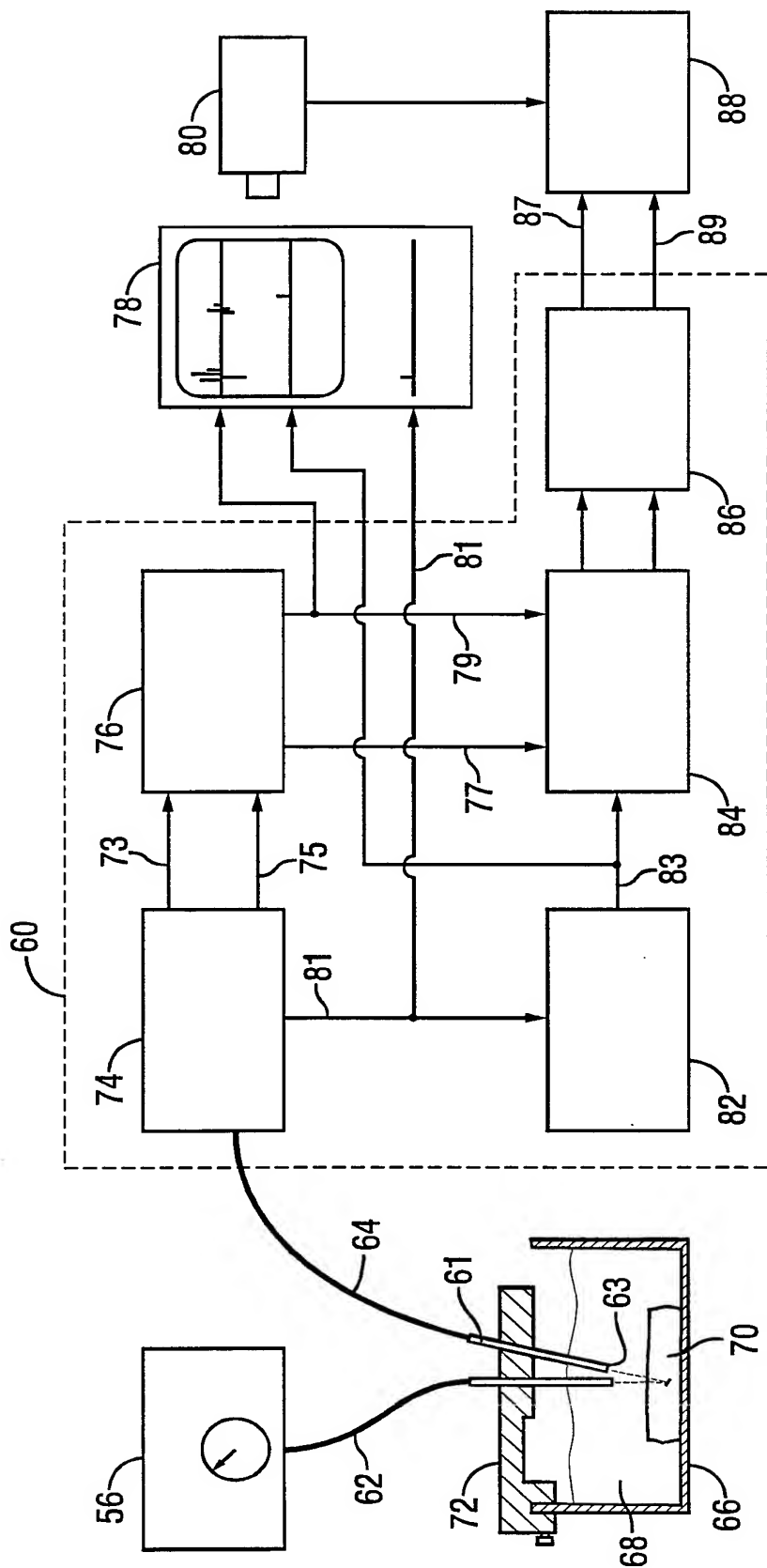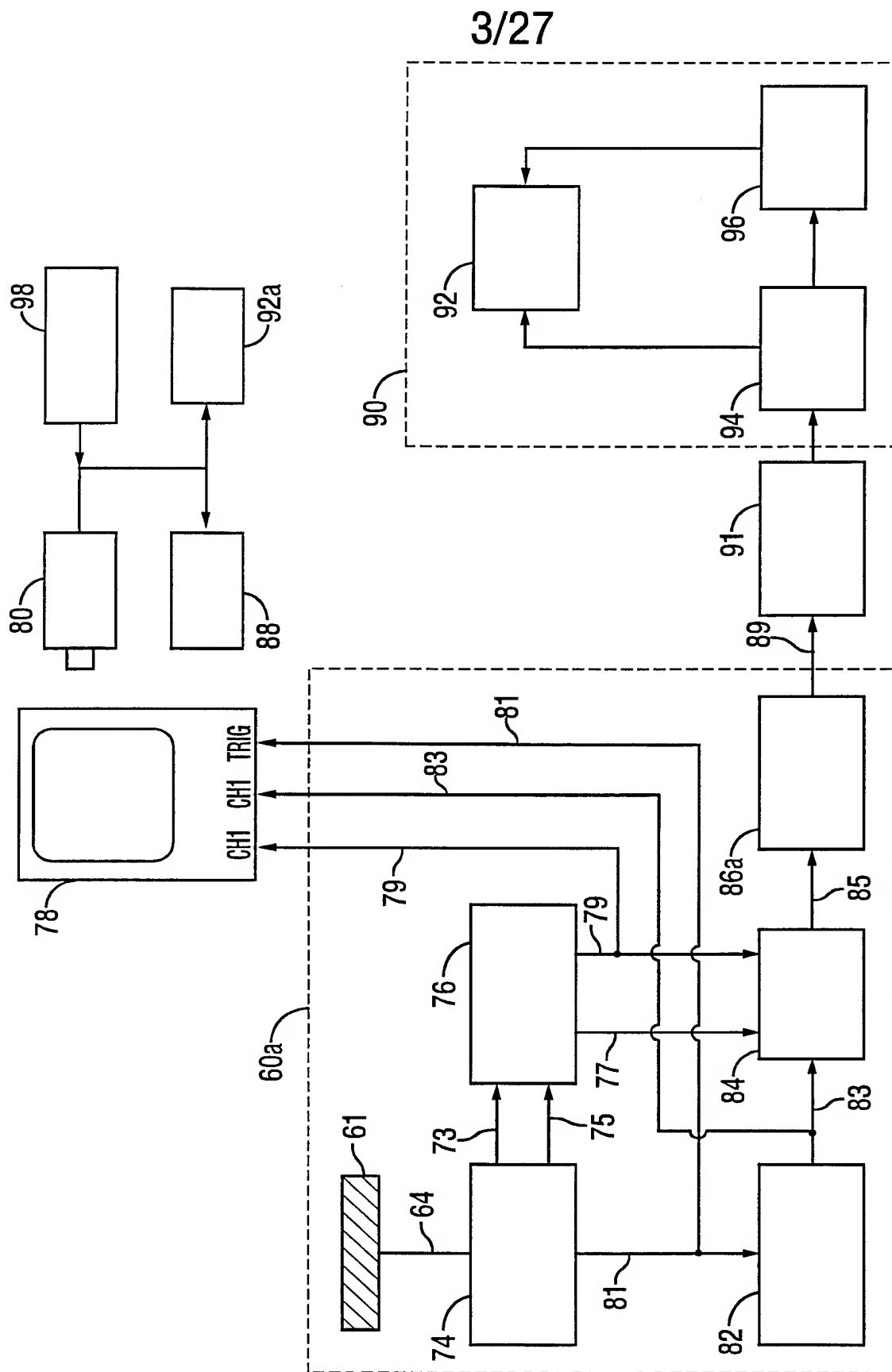
FIG. 2a

4/27

FIG.3

FIG.3A
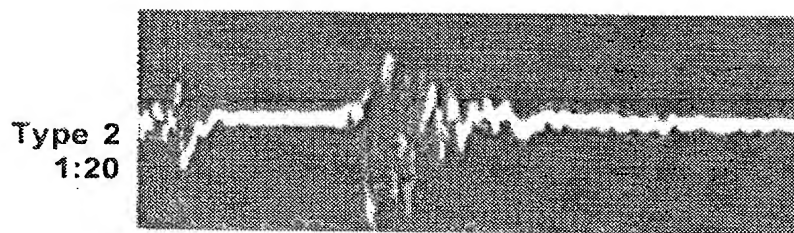
FIG.3B
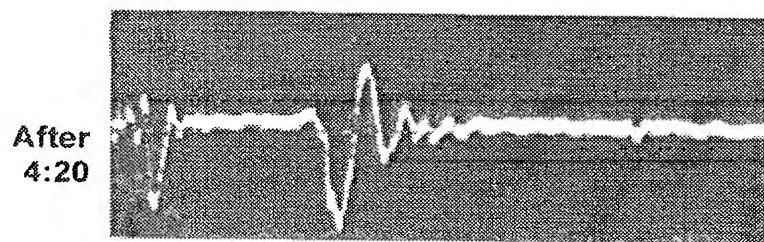
FIG.3C
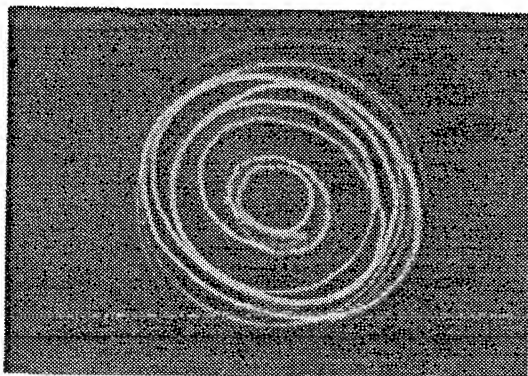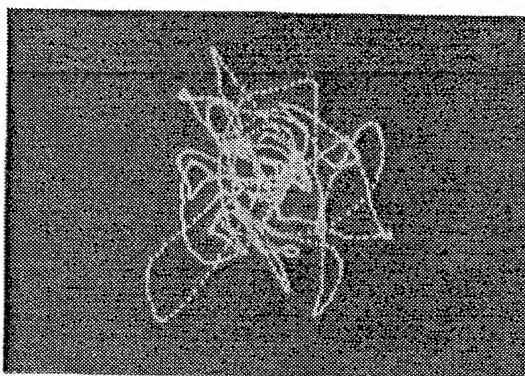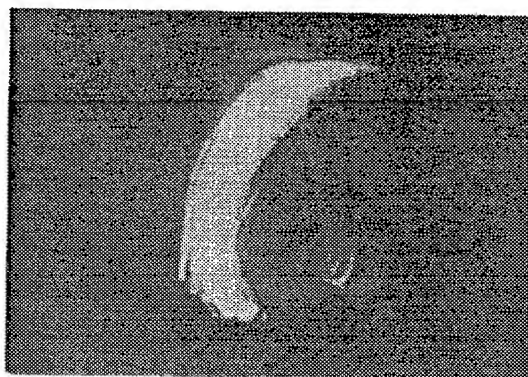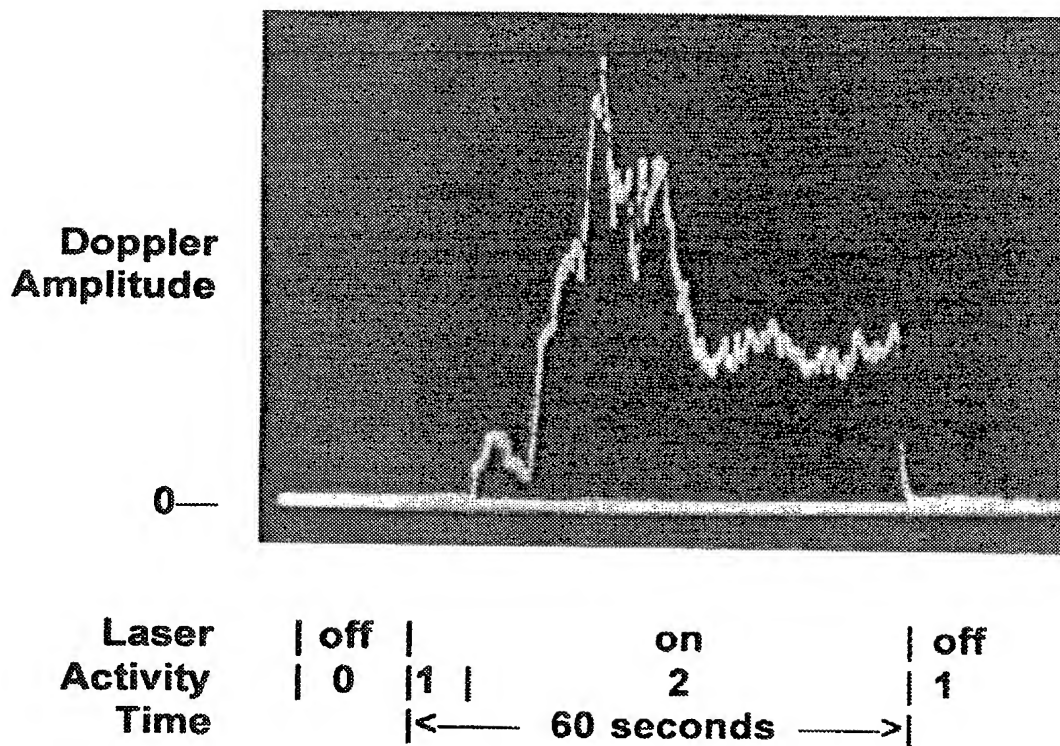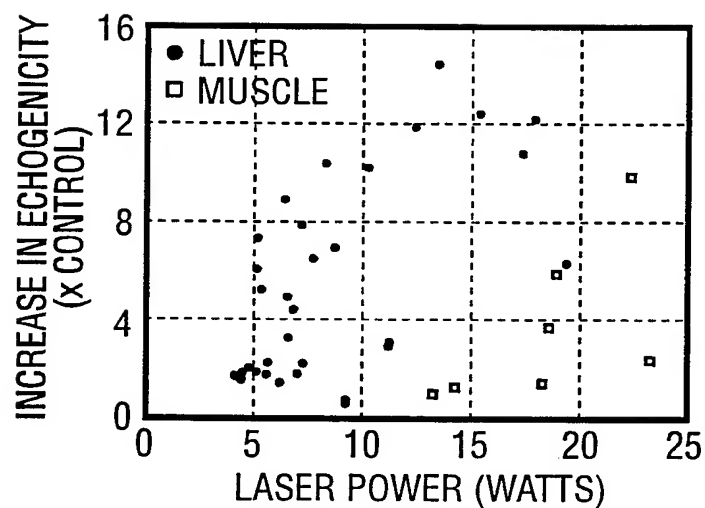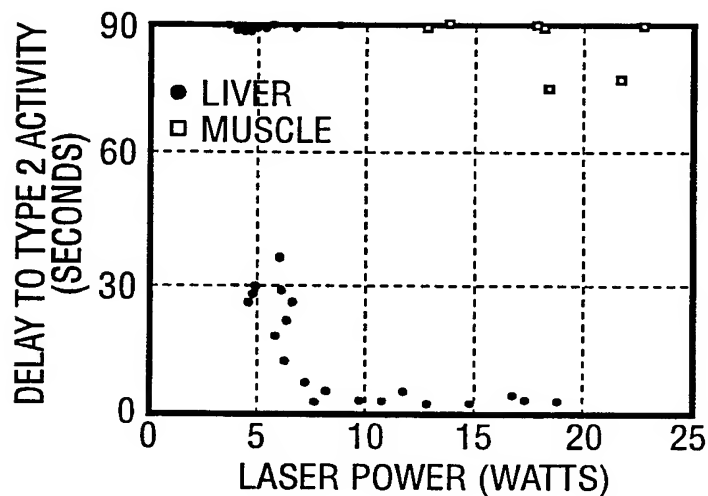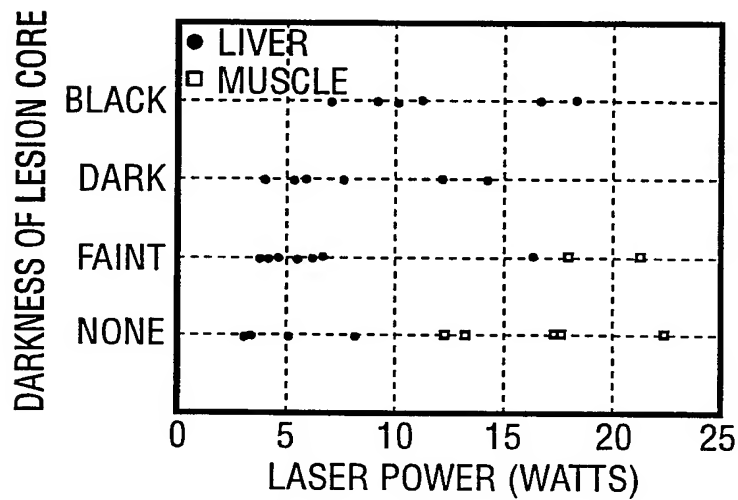
FIG.4

FIG.4A

FIG.4B

Doppler Amplitude

0—

Laser		off			on		off
Activity		0	|1		2		1
Time				<——— 60 seconds ———>			

FIG.5

FIG. 6

FIG. 6a

FIG. 6b

FIG. 7

FIG. 7a

FIG. 8

Ch1:origin=(-2.009, 0.0968)

Ch2:origin=(-0.1385, 0.1124)

FIG. 9

FIG. 9a

Ch3:origin=(0.506, 0.1438)

Ch4:origin=(0.4128, 0.08791)

FIG. 9b

FIG. 9c

Ch5:origin=(-0.1087, -1.019)

Ch6:origin=(-0.8409, -0.7727)

FIG. 9d

FIG. 9e

Ch7:origin=(-1.079, 0.02796)

Ch8:origin=(0.2036, 0.6061)

FIG. 9f

FIG. 9g

12/27

FIG. 10

Ch1

FIG. 10a

Ch2

FIG. 10b

Ch3

FIG. 10c

Ch4

FIG. 10d

Ch5

FIG. 10e

Ch6

FIG. 10f

Ch7

FIG. 10g

Ch8
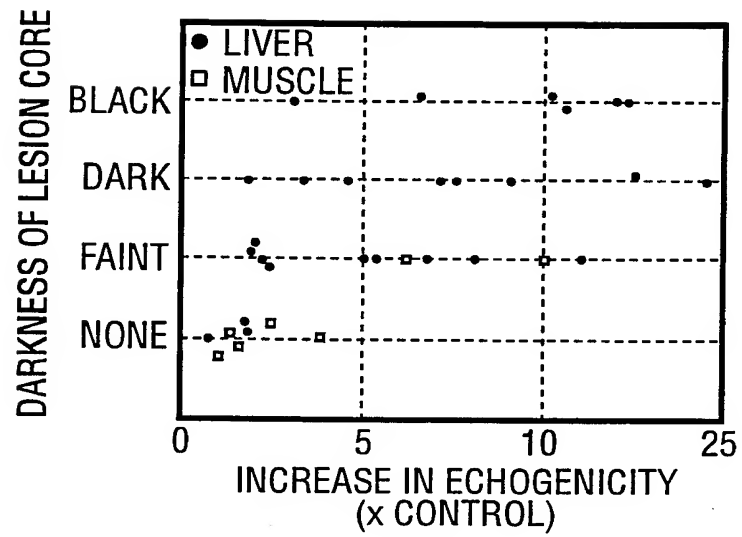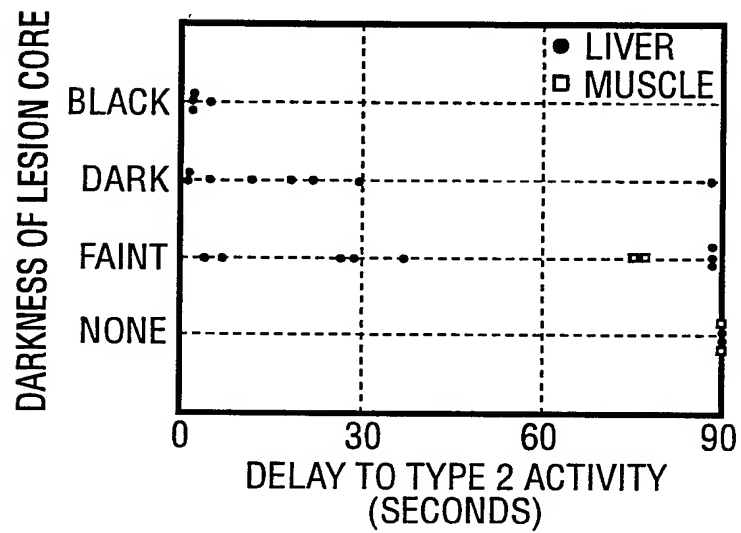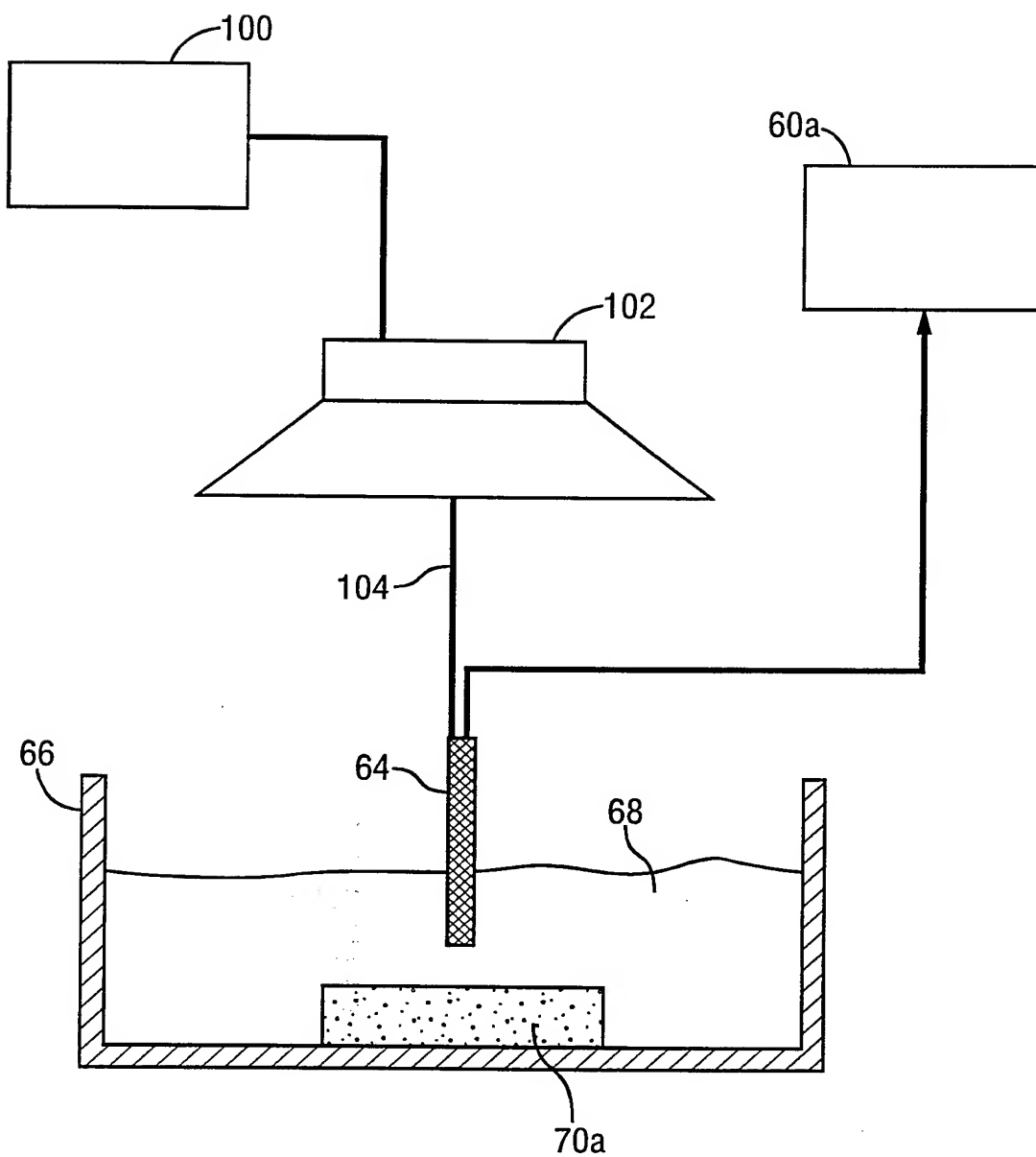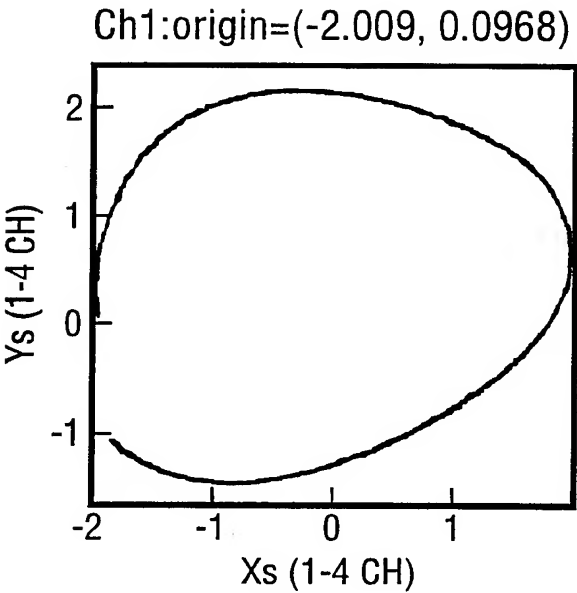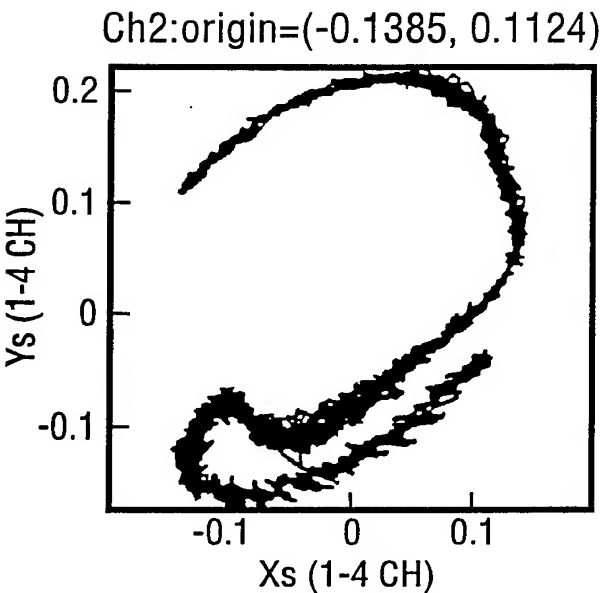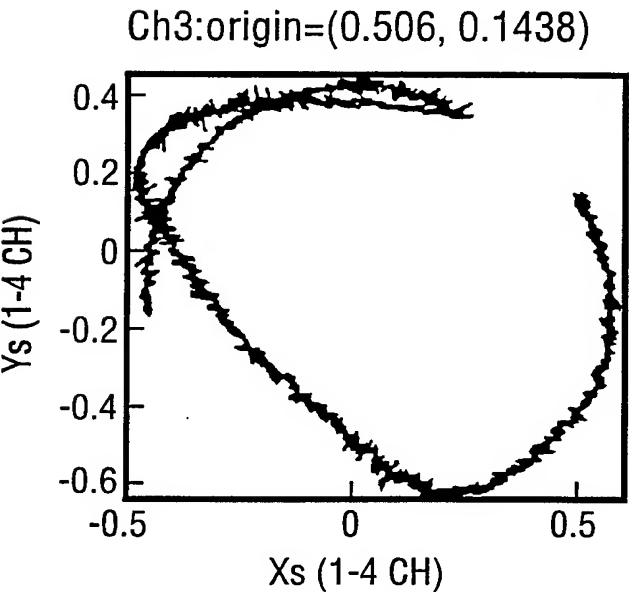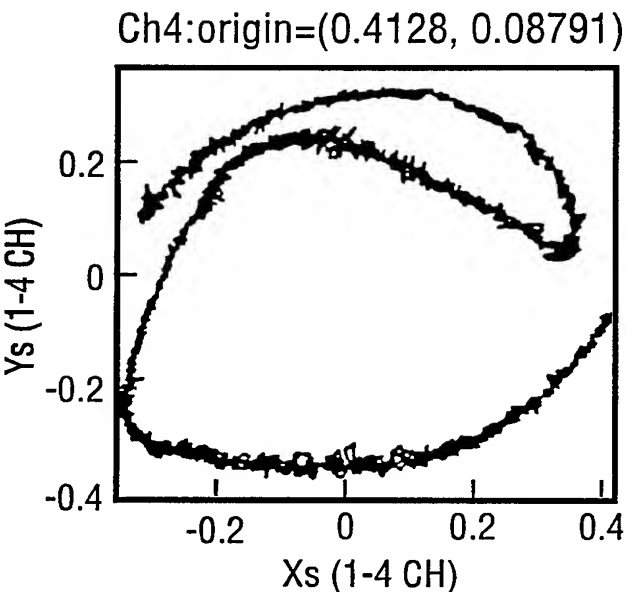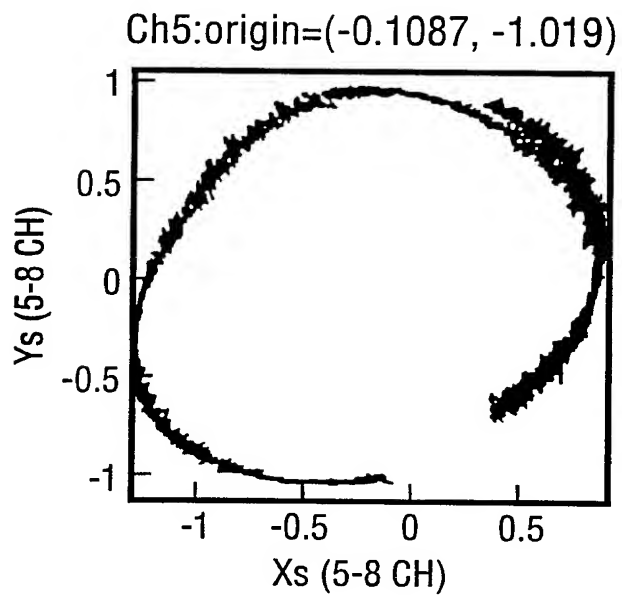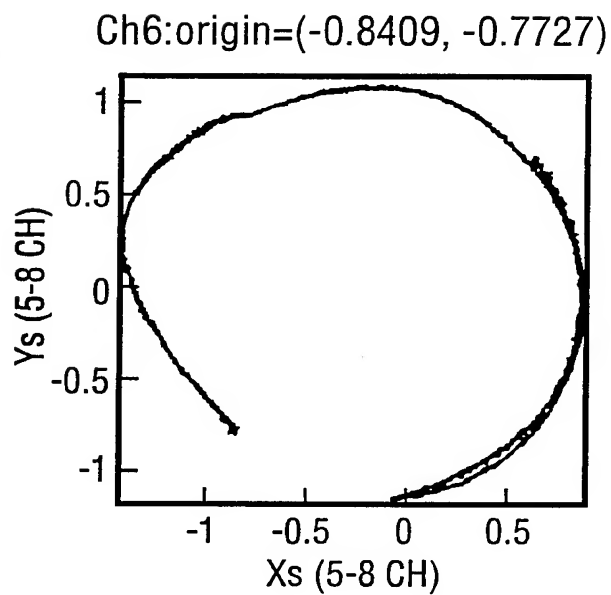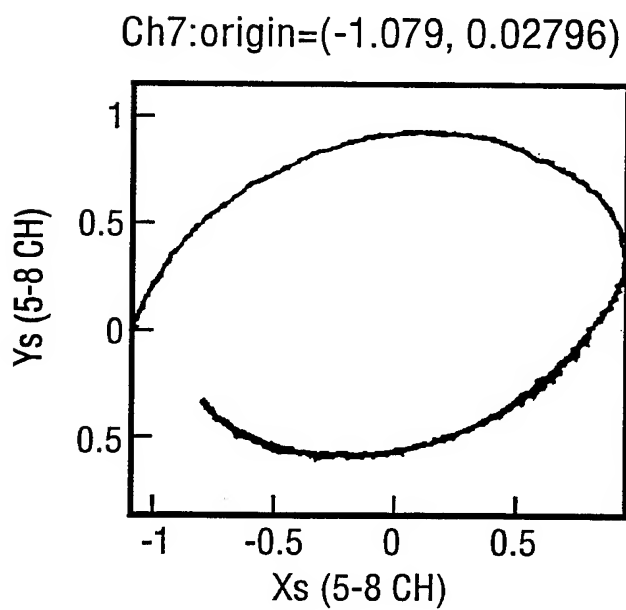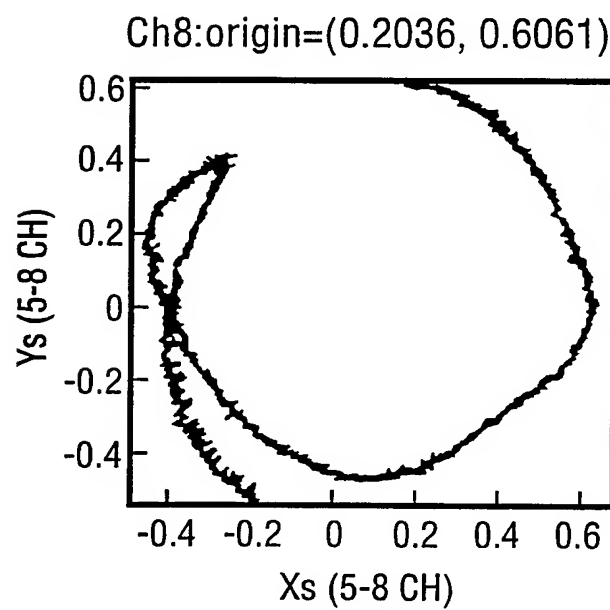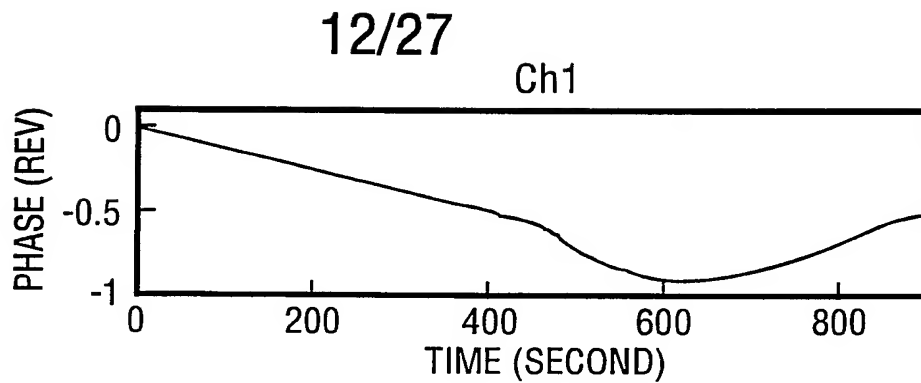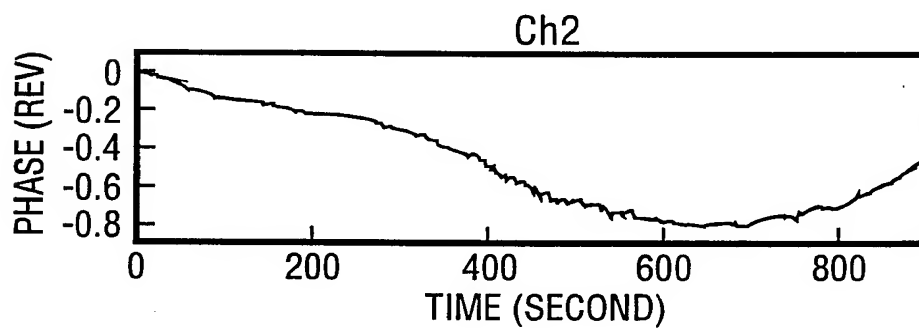
FIG. 11

Ch1:origin=(-0.2912, 0.3115)

FIG. 12

Ch2:origin=(-0.001069, 0.8001)
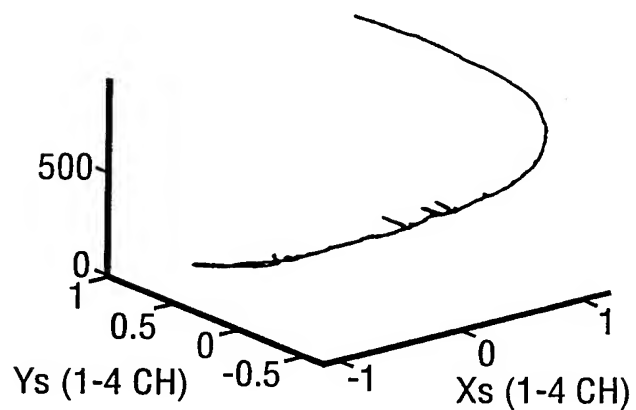
FIG. 12a

Ch3:origin=(1.684, -0.9338)
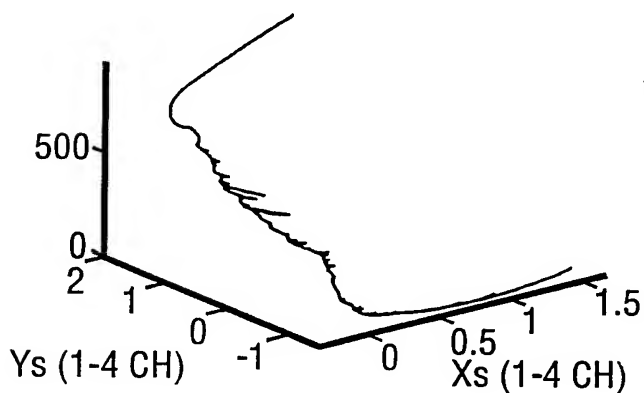
FIG. 12b

Ch4:origin=(1.2, -0.4146)
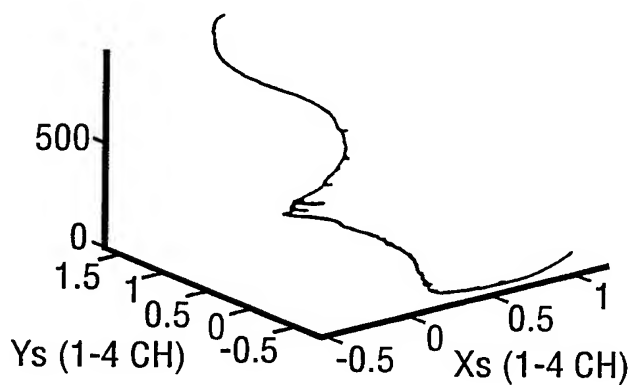
FIG. 12c

Ch5:origin=(-0.5626, 0.6974)
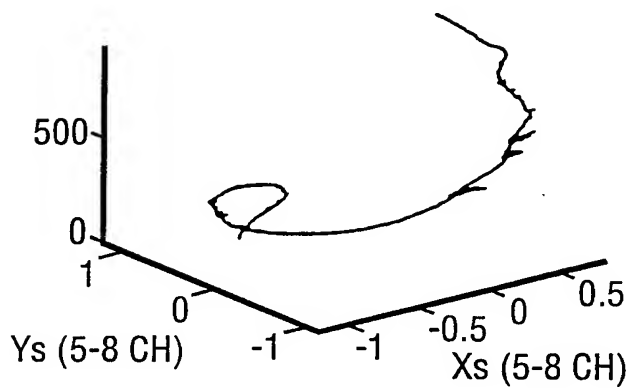
FIG. 12d

Ch6:origin=(1.015, -0.1231)
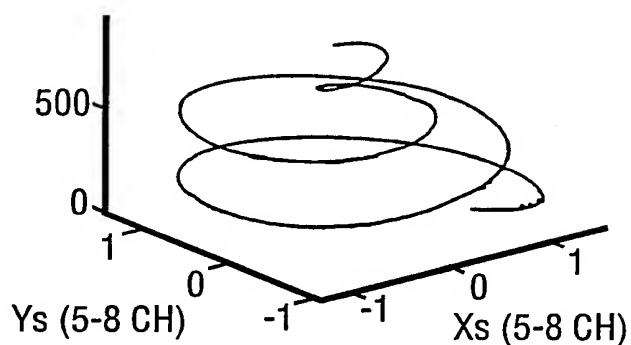
FIG. 12e

Ch7:origin=(-0.06552, -0.04895)
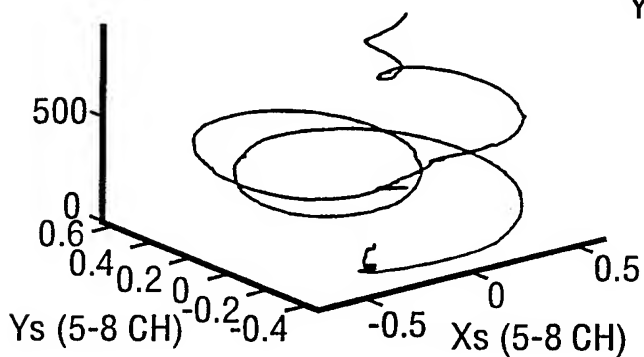
FIG. 12f

Ch8:origin=(0.3079, 0.02931)
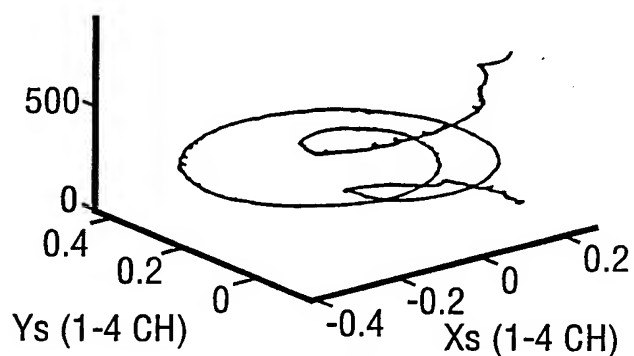
FIG. 12g

Ch1:origin=(-0.4906, 0.2387)
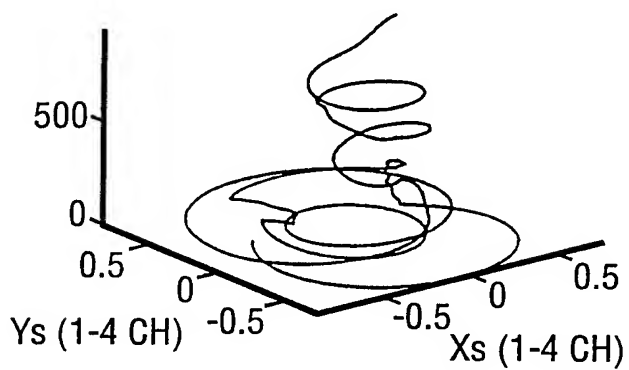
FIG. 13

Ch2:origin=(-0.06565, -0.05914)
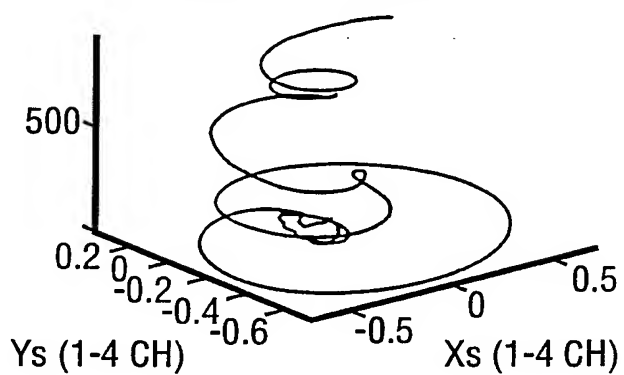
FIG. 13a

Ch3:origin=(0.1246, 0.1044)
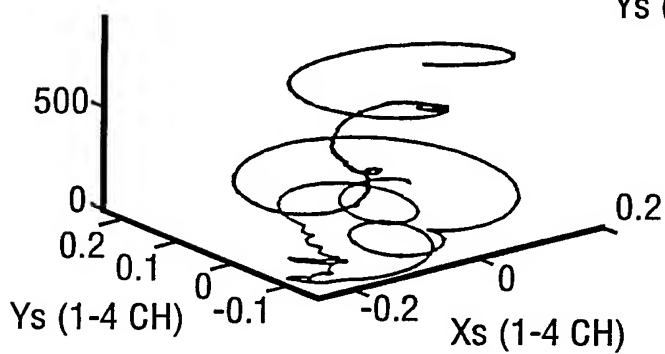
FIG. 13b

Ch4:origin=(0.1164, 0.07197)
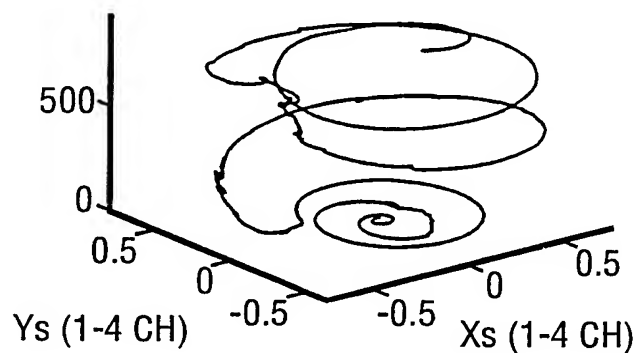
FIG. 13c

Ch5:origin=(0.4143, 0.2677)
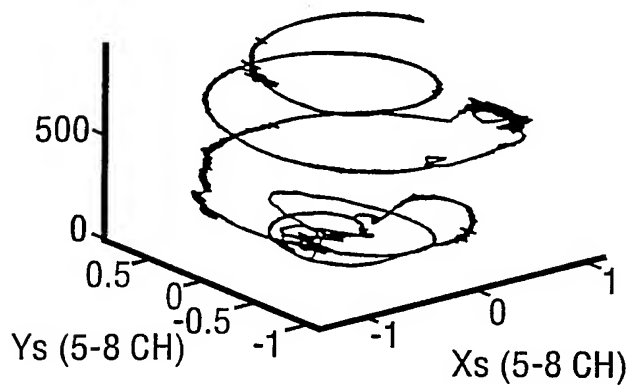
FIG. 13d

Ch6:origin=(0.03054, -0.6456)
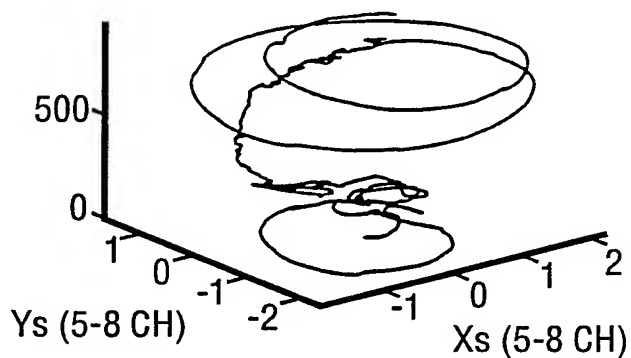
FIG. 13e

Ch7:origin=(-0.06717, 0.09586)
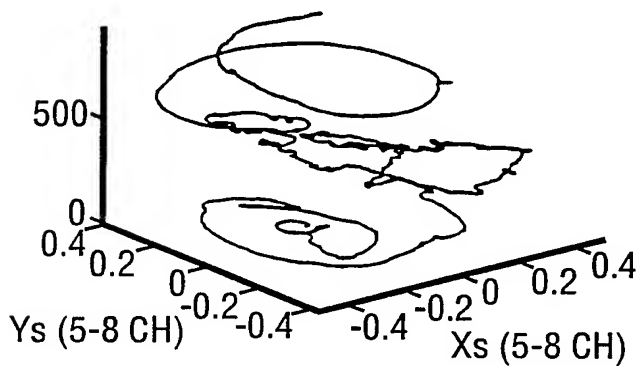
FIG. 13f

Ch8:origin=(-0.01223, -0.0579)

FIG. 13g

FIG. 14
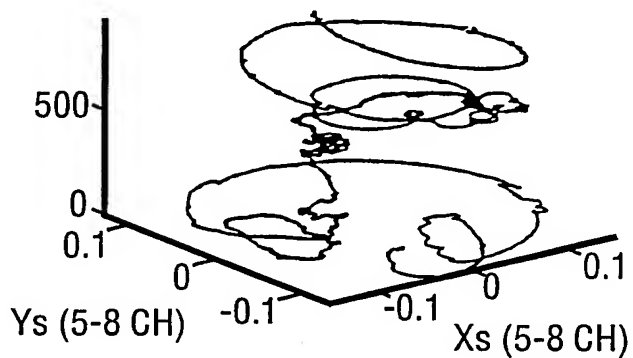
Ch1:origin=(0.3595, 0.02147)
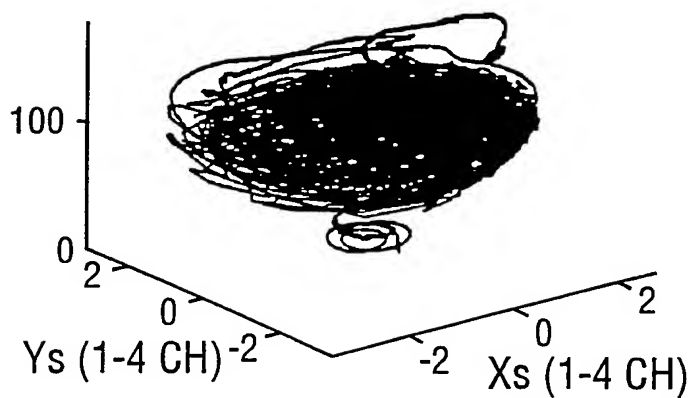
FIG. 15

Ch2:origin=(-0.6579, 0.2457)
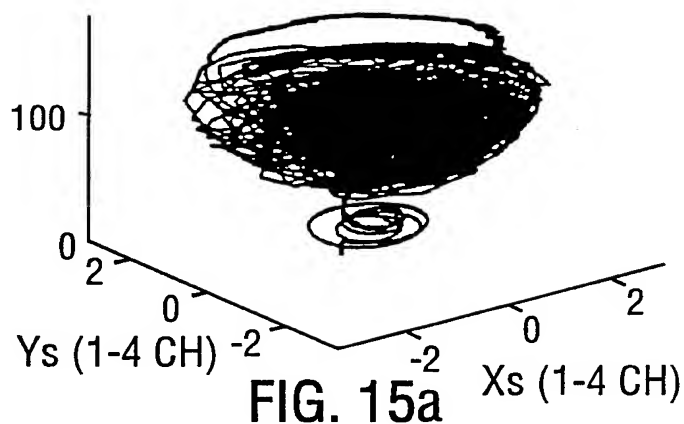
FIG. 15a

Ch3:origin=(0.312, 0.9584)
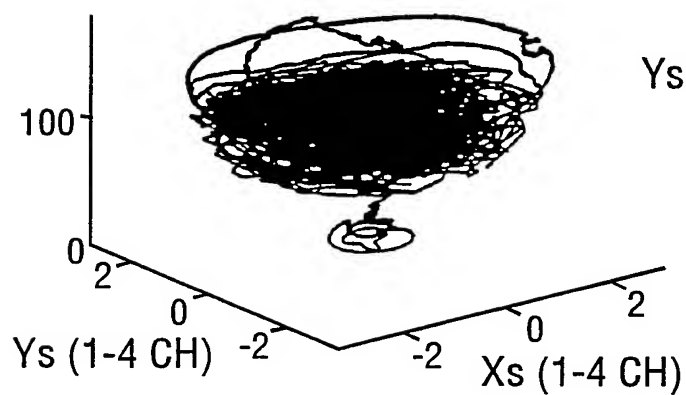
FIG. 15b

Ch4:origin=(-0.09238, 0.217)
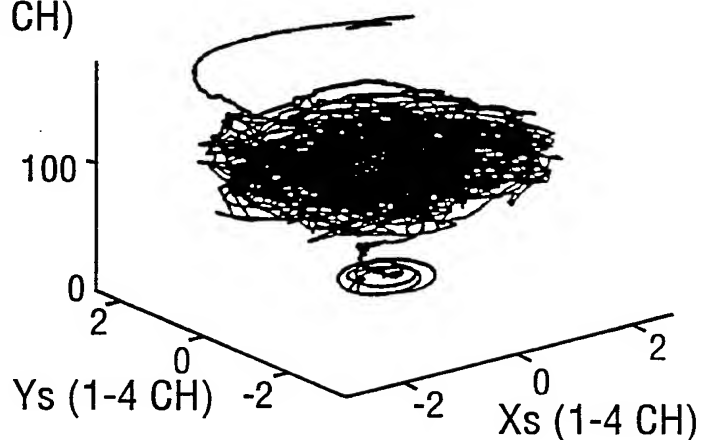
FIG. 15c

Ch5:origin=(0.1484, -0.5773)
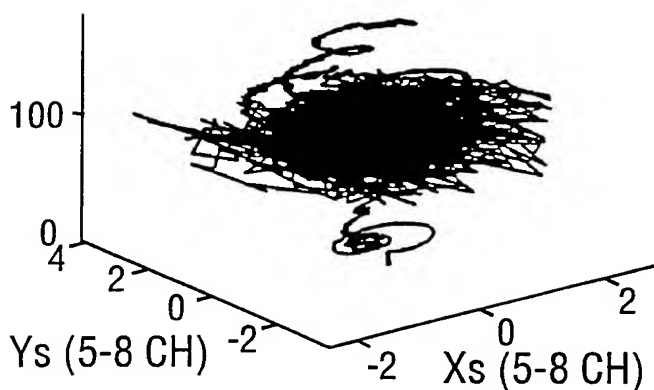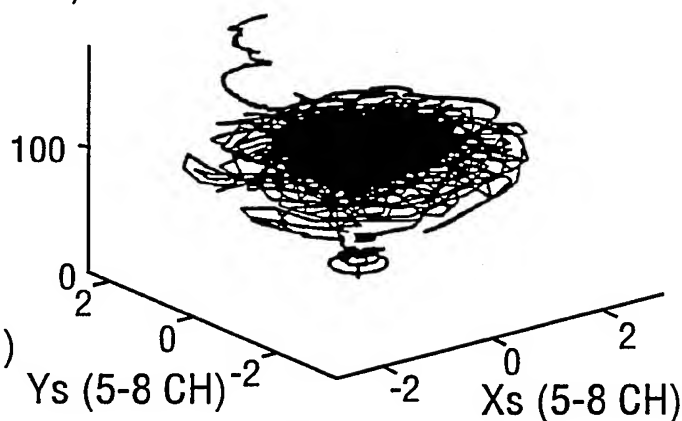

FIG. 15d

Ch6:origin=(0.1219, -01717)

FIG. 15e

Ch7:origin=(0.469, -0.2409)
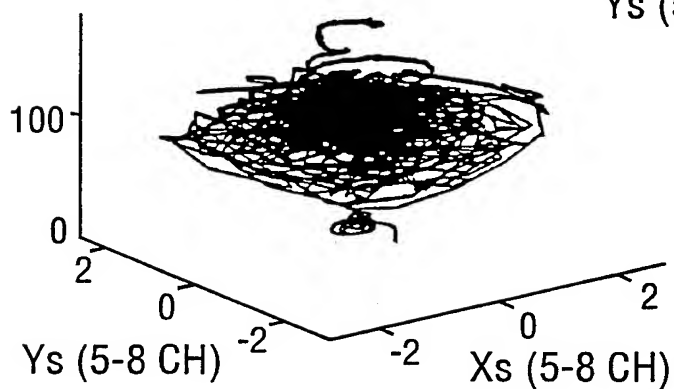
FIG. 15f

Ch8:origin=(-0.01924, -0.2035)

FIG. 15g

FIG. 16
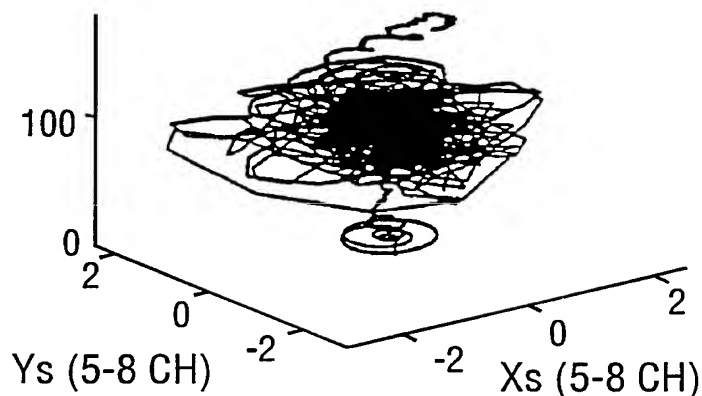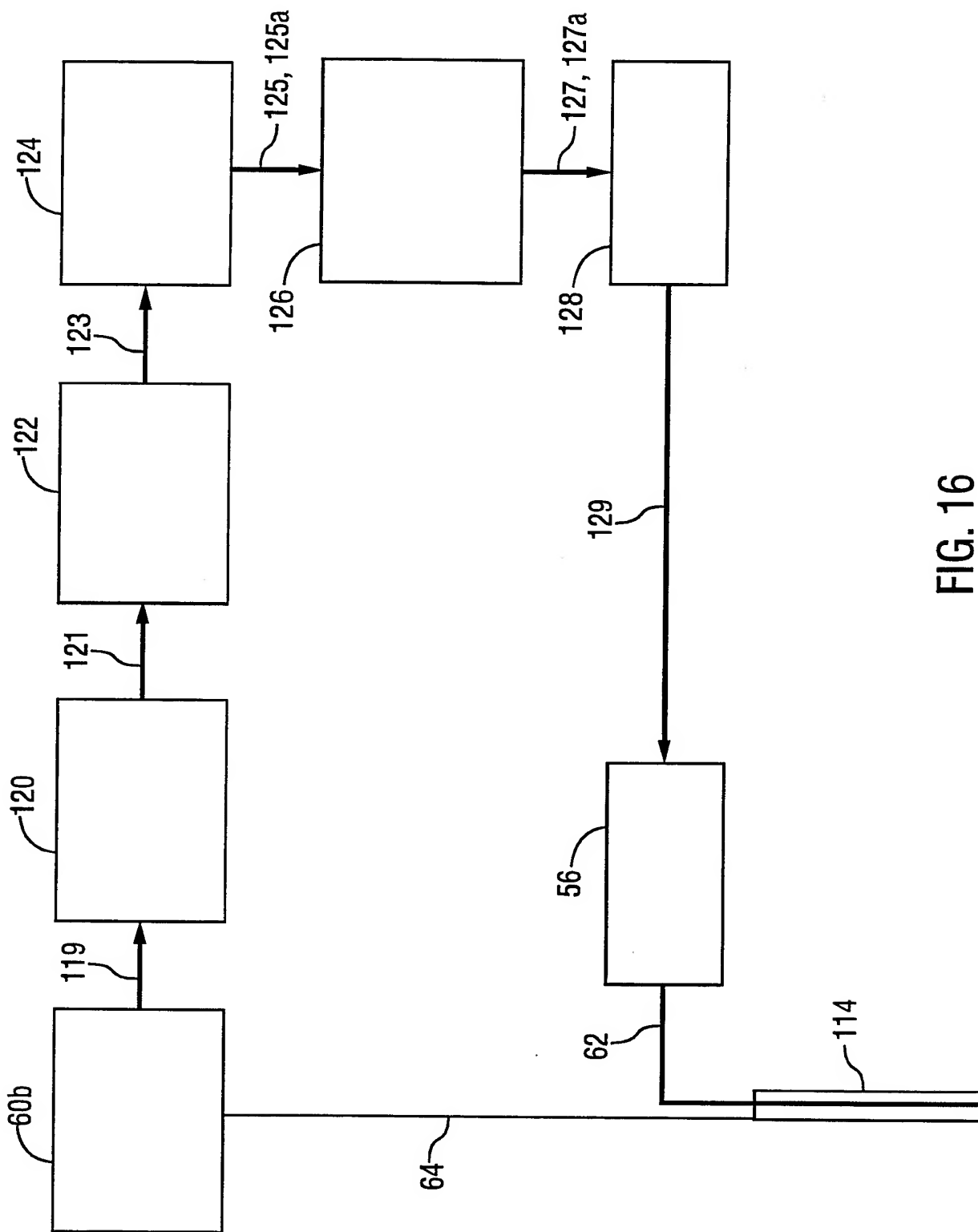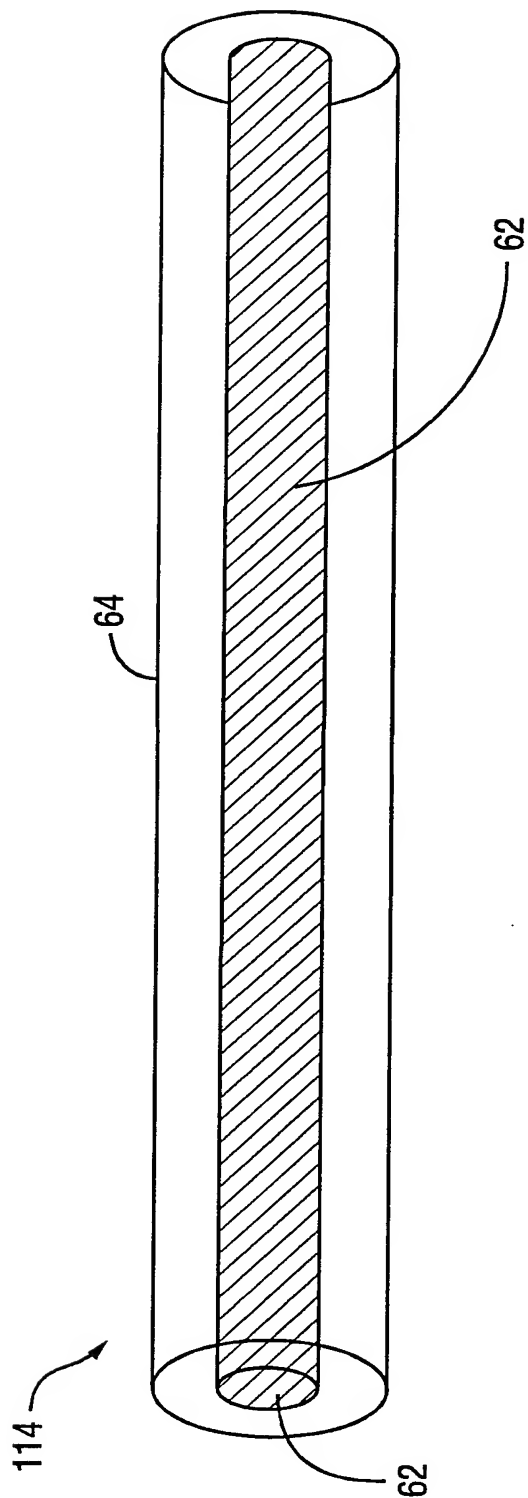
62

64

62

114

FIG. 17

FIG. 18

FIG. 19

26/27

FIG. 20
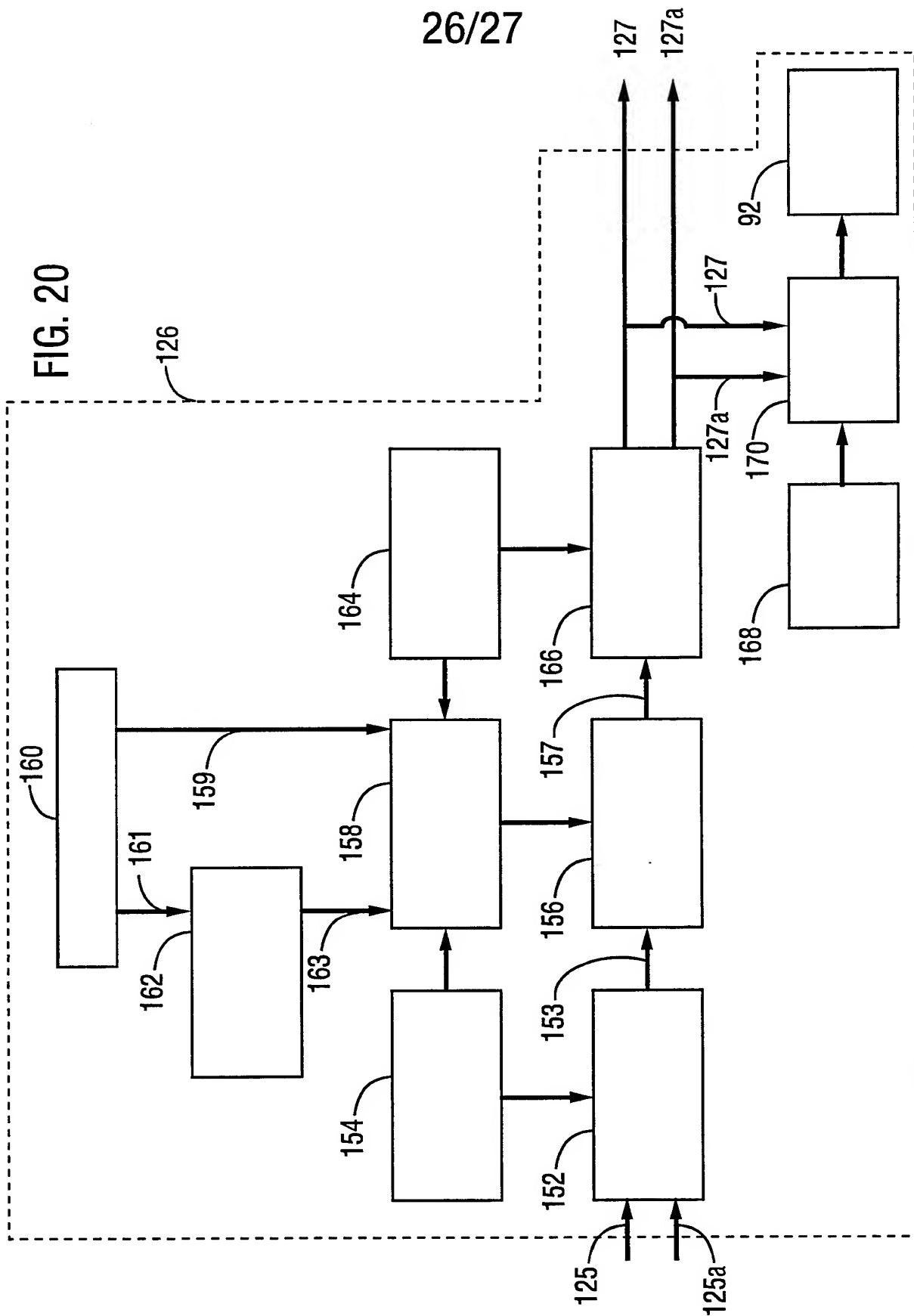
27/27

FIG. 21

INTERNATIONAL SEARCH REPORT

A. CLASSIFICATION OF SUBJECT MATTER
IPC 6   A61N7/02   A61B8/08

According to International Patent Classification (IPC) or to both national classification and IPC

B. FIELDS SEARCHED

Minimum documentation searched (classification system followed by classification symbols)
IPC 6   A61N   A61B

Documentation searched other than minimum documentation to the extent that such documents are included in the fields searched

Electronic data base consulted during the international search (name of data base and, where practical, search terms used)

C. DOCUMENTS CONSIDERED TO BE RELEVANT

Category°	Citation of document, with indication, where appropriate, of the relevant passages	Relevant to claim No.
A	EP,A,0 162 735 (DORY) 27 November 1985 see abstract; claim 1 see page 1, line 6 - page 2, line 26 ---	1,2,6-8, 13
A	EP,A,0 484 619 (HEWLETT-PACKARD) 13 May 1992 see abstract; claim 1 ---	1,7
A	EP,A,0 430 093 (ACOUSTIC IMAGING) 5 June 1991 see abstract ---	1,7
A	US,A,5 088 498 (BEACH) 18 February 1992 see abstract see column 3, line 61 - column 5, line 50 --- -/--	1,7

| [X] | Further documents are listed in the continuation of box C. | [X] | Patent family members are listed in annex. |

° Special categories of cited documents :

"A" document defining the general state of the art which is not considered to be of particular relevance

"E" earlier document but published on or after the international filing date

"L" document which may throw doubts on priority claim(s) or which is cited to establish the publication date of another citation or other special reason (as specified)

"O" document referring to an oral disclosure, use, exhibition or other means

"P" document published prior to the international filing date but later than the priority date claimed

"T" later document published after the international filing date or priority date and not in conflict with the application but cited to understand the principle or theory underlying the invention

"X" document of particular relevance; the claimed invention cannot be considered novel or cannot be considered to involve an inventive step when the document is taken alone

"Y" document of particular relevance; the claimed invention cannot be considered to involve an inventive step when the document is combined with one or more other such documents, such combination being obvious to a person skilled in the art.

"&" document member of the same patent family

Date of the actual completion of the international search	Date of mailing of the international search report
7 August 1995	3 1. 08. 95

Name and mailing address of the ISA	Authorized officer
European Patent Office, P.B. 5818 Patentlaan 2 NL - 2280 HV Rijswijk Tel. (+31-70) 340-2040, Tx. 31 651 epo nl, Fax: (+31-70) 340-3016	Taccoen, J-F

1

C.(Continuation) DOCUMENTS CONSIDERED TO BE RELEVANT

Category°	Citation of document, with indication, where appropriate, of the relevant passages	Relevant to claim No.
A	NL,A,7 710 433 (HOFFMAN-LAROCHE) 10 April 1978 see claim 1	1,7
A	FR,A,2 367 293 (HOFFMANN-LAROCHE) 5 May 1978 see claim 1	1,7
A	FR,A,1 497 496 (MASSIOT PHILIPS) 13 October 1967 see claim 1	1,7
A	GB,A,2 113 099 (VILKOMERSON) 3 August 1983 see abstract	1,7
P,A	WO,A,95 01125 (INSTITUTE OF CANCER RESEARCH.) 12 January 1995 see abstract	1,7
P,A	WO,A,95 01126 (INSTITUTE OF CANCER RESEARCH) 12 January 1995 see page 1, line 1 - page 2, line 3 see page 3, line 24 - page 5, line 5 see page 7, line 6 - line 23	1,7

1

INTERNATIONAL SEARCH REPORT

information on patent family members

Patent document cited in search report	Publication date	Patent family member(s)		Publication date
EP-A-0162735	27-11-85	FR-A-	2563725	08-11-85
		DE-A-	3585691	23-04-92
		EP-A,B	0339693	02-11-89
		JP-C-	1765452	11-06-93
		JP-B-	4035181	10-06-92
		JP-A-	60241436	30-11-85
		US-A-	5143073	01-09-92
		US-E-	RE33590	21-05-91
		US-A-	5080102	14-01-92
		US-A-	5111822	12-05-92
		US-A-	5080101	14-01-92
		US-A-	5150712	29-09-92
		US-A-	4658828	21-04-87
EP-A-0484619	13-05-92	US-A-	5103824	14-04-92
		JP-A-	4282144	07-10-92
		US-A-	5195521	23-03-93
EP-A-0430093	05-06-91	JP-A-	4002336	07-01-92
		US-A-	5188112	23-02-93
		US-A-	5170792	15-12-92
US-A-5088498	18-02-92	US-A-	5183046	02-02-93
		US-A-	5289820	01-03-94
NL-A-7710433	10-04-78	US-A-	4143650	13-03-79
		CH-A-	625409	30-09-81
		DE-A-	2745063	13-04-78
		FR-A,B	2367293	05-05-78
		GB-A-	1592695	08-07-81
		JP-A-	53046188	25-04-78
		JP-B-	63006214	08-02-88
FR-A-2367293	05-05-78	US-A-	4143650	13-03-79
		CH-A-	625409	30-09-81
		DE-A-	2745063	13-04-78
		GB-A-	1592695	08-07-81
		JP-A-	53046188	25-04-78
		JP-B-	63006214	08-02-88
		NL-A-	7710433	10-04-78

INTERNATIONAL SEARCH REPORT

Information on patent family members

Patent document cited in search report	Publication date	Patent family member(s)		Publication date
FR-A-1497496	02-01-68	NONE		
GB-A-2113099	03-08-83	DE-A-	3300121	14-07-83
WO-A-9501125	12-01-95	GB-A-	2279743	11-01-95
WO-A-9501126	12-01-95	GB-A-	2279742	11-01-95

Form PCT/ISA/210 (patent family annex) (July 1992)